



*Facultad  
de  
Ciencias*

**ESTUDIO DE DIFERENTES  
MECANISMOS DE TRANSICIÓN  
METAL/AISLANTE EN SÓLIDOS**  
(Study of different mechanisms for  
metal/insulator transitions in solids)

Trabajo de Fin de Grado  
para acceder al

**GRADO EN FÍSICA**

**Autor: Marta Sainz de la Maza Cantero**

**Director: Francisco Javier Junquera Quintana**

**Junio - 2017**



# Resumen

El presente documento forma parte del último curso del Grado en Físicas. El objetivo general de este trabajo es reforzar algunos conocimientos adquiridos durante el grado.

El objetivo específico de este trabajo era estudiar tres mecanismos de transición metal a aislante: la transición de Mott a través del hamiltoniano de Hubbard, la transición de Peierls debida a dimerización y deformaciones elásticas de átomos y la transición de Anderson, causada por impurezas en los materiales. Solo se ha podido estudiar la transición de Mott debido a que se han obtenido resultados inesperados dependiendo de la dimensionalidad del problema. En principio, se esperaba obtener una transición de Mott independientemente de si el sistema de estudio era 1D, 2D o 3D, sin embargo esta transición no se obtiene para problemas 1D que son los estudiados en este trabajo. Finalmente, se han reproducido dos cadenas lineales, una ferromagnética y otra antiferromagnética, con estados  $1s$  en cada sitio de red, dando información detallada de las bandas electrónicas y las densidades de estado. Después, ambas cadenas se han caracterizado bajo diferentes condiciones iniciales. Las simulaciones se han realizado a través de un código basado en segundos principios según el modelo de enlace fuerte.

Además, se ha incluido en el presente trabajo otra transición llamada localización dinámica. Esta modificación en el proyecto es debida a la concesión de una beca para realizar una estancia en la Universidad de Brown. El trabajo realizado durante la estancia debía ser incluido en el trabajo de fin de grado. La transición debida a localización dinámica aparece cuando se reproduce el modelo de enlace fuerte con campo eléctrico dependiente del tiempo. Dependiendo de cuales sean los valores de intensidad y frecuencia del campo eléctrico, se puede obtener un material aislante.



## Abstract

This document is part from the last course of the degree in Physics. The general aim of this work is to reinforce the knowledges acquired during the degree.

The specific goal of this work was to study three mechanism for transitions metal-to-insulator: the Mott transition through the Hubbard hamiltonian, the Peierls transition due to dimerization of atoms and elastic deformations and the Anderson transition caused by the presence of impurities. Only the Mott transition has been reproduced due to the unexpected results in relation with the dimensionality of the problem. Initially, a Mott transition was expected independently of having a 1D, 2D or 3D systems, but this transition is not observed in 1D problems which are solved here. This behavior has been analyzed in depth so it took more time than firstly planned. Finally, simulations of a ferromagnetic and antiferromagnetic linear chains with only a  $1s$  state per lattice site have been done giving a detailed information of the shape of its electronic bands and density of states. Then, both systems have been characterized under different initial conditions. Simulations have been solved with a simple second-principle method based on tight-binding model.

Moreover, other transition was added to this document called dynamical localization. Such modification in this project arise from the concession of a scholarship to spend two months at Brown University. The work done in this stance should be part of this undergraduate thesis. Dynamical localization transition is caused by the introduction of a time-dependent electric field into a tight-binding model. An insulator emerges for certain values of the intensity and frequency of the electric field.

**Keywords:** tight-binding model, Hubbard model, Mott transition, second-principle methods, time-dependent electric-field, dynamical localization.



# Table of contents

<b>1</b>	<b>Introduction</b>	<b>1</b>
1.1	First-principle methods . . . . .	1
1.2	Second-principle methods . . . . .	2
1.3	Structure of this work . . . . .	2
<b>2</b>	<b>Tight-binding model</b>	<b>5</b>
2.1	The secular equation . . . . .	6
2.2	Hamiltonian and overlap matrix . . . . .	9
2.2.1	Hamiltonian matrix elements . . . . .	9
2.2.2	Overlap matrix elements . . . . .	10
2.3	Tight-binding bands . . . . .	11
2.4	Conclusions . . . . .	14
<b>3</b>	<b>The Hubbard model</b>	<b>15</b>
3.1	The Hubbard Hamiltonian . . . . .	16
3.2	Shape of the electronic bands and density of states . . . . .	17
3.3	Ferromagnetic chain . . . . .	22
3.4	Antiferromagnetic chain . . . . .	25
3.5	Transition diagrams . . . . .	26
3.6	Conclusions . . . . .	28

<b>4</b>	<b>Tight-binding model under an external electric field</b>	<b>29</b>
4.1	Time-dependent electric fields . . . . .	29
4.1.1	Time-dependent Hamiltonian . . . . .	29
4.1.2	Floquet formalism . . . . .	32
4.2	Tight-binding model in a time-periodic electric field . . . . .	33
4.3	Results . . . . .	35
4.4	Conclusions . . . . .	38
	<b>References</b>	<b>41</b>
	<b>Appendix A Demonstrations</b>	<b>43</b>
A.1	Proof that the basis functions defined in Eq.(2.7) verify the Bloch theorem . . . . .	43
A.2	Derivation the factor $A_{\mu\vec{k}}$ required for the Bloch basis states $\phi_{\mu\vec{k}}(\vec{r})$ to be normalized. . . . .	44
A.3	Proof that the Bloch basis functions are orthonormal if the orbitals centered in different atoms are orthonormal . . . . .	46
A.4	Demonstration of the Floquet matrix $H_{mn} - n\Omega\delta_{mn}$ . . . . .	47
	<b>Appendix B Computational equations</b>	<b>51</b>
B.1	Tight-binding equations . . . . .	51
B.1.1	One atom per unit cell . . . . .	56
B.1.2	Two atoms per unit cell . . . . .	57
B.2	Hubbard model equations . . . . .	58
B.3	Self-consistent equations . . . . .	60
	<b>Appendix C Comparison of the energies for converged systems with occupation <math>n_l^\sigma \neq 0.5</math></b>	<b>63</b>

# Chapter 1

## Introduction

Nowadays many properties of materials are directly obtained from the fundamental equations to provide new insights into real problems in physics, chemistry and material science. Electronic structure calculations are becoming tools used by both experimentalists and theorists to understand characteristic properties of matter. These calculations could be solved with different computational methods which include some approaches, e.g. the Born-Oppenheimer approximation, in order to be able to solve huge equations with a reasonable computational cost. A first-principles method is one which does not make assumptions or use empirical model or parameter fitting to solve the fundamental equations. A first-principles-based, or second-principles, is a method that permits large-scale materials simulations with a modest computational cost because some approximations or parameter fitting are done. These methods are usually iterative methods where the density of electrons of each level of energy is guessed in the first step.

### 1.1 First-principle methods

Although in this work no first-principle methods are used, it is convenient and useful to know which schemes these methods are based on and which are their limitations.

Let's start from the Schrödinger equation. If one wants to reproduce the electronic structure of a system where nucleus and electrons are involved, for a non-relativistic scheme, the Schrödinger equation must be solved. However, this equation is very difficult and it can only be solved analytically for a two-particle system, the  $H_2$  molecule. Far from  $N = 2$ , for a very few particles, could be solved numerically. For systems where many particles are enrolled, a set of "accepted" approximations should be done, keeping the method as first-principles. Typical approaches are the Born-Oppenheimer approximation for decoupling the movement of the electrons and nucleus, the density functional theory to treat the electron-electron interactions, pseudopotentials to treat the

nuclei + core electrons, basis set to expand the eigenstates of the hamiltonian and supercells to deal with periodic systems.

However, sometimes, these approximations are not enough to reproduce experiments, for example, because are reproduced at ambient temperature, under applied time-dependent external field, out of equilibrium, etc. These conditions cause the system not to be under periodic conditions so, to be able to reproduce its behavior, many particles should be included explicitly in the calculus and, even computationally, its extremely cost. In this case, second-principle methods must be used.

## 1.2 Second-principle methods

In this work, a second-principles method is used to solve two widely known problems: the tight-binding model and the Hubbard model. For the simulations of this first two chapters, a code called SCALE-UP was used.

The aim of second-principles methods is to parametrize some difficult interactions between electrons given by huge integrals in first-principles methods. Through parametrization, bigger systems can be reproduced with second-principles methods. The procedure followed in a real work should include a simulation of the material with some method based in first-principles from where the values of these integrals are obtained. Then these values are translated to second-principles.

In this work different systems under different values of two parameters have been studied, so they are not given by first-principles. These two parameters are the hopping integral,  $\gamma$ , and the coulomb interaction,  $U$ . Moreover the density of states,  $n_l^\sigma$  with  $l$  a given lattice site and  $\sigma$  each spin flavor, is also changed. The value of  $n_l^\sigma$  does not come from first-principles but is calculated on each step of iteration. In Appendix B, a more detailed description of the iteration steps can be consulted.

## 1.3 Structure of this work

This work include three main chapters:

1. In Chapter 2 a tight binding model is reproduced for three different systems: a 1D, 2D and 3D systems with only a  $s$  state in each lattice site. Here, only the hopping parameter  $\gamma$  appears, so it is shown how are the characteristics of electronic bands and density of states depending on this value.
2. In Chapter 3 Hubbard model is applied to a linear chain. The hamiltonian which governs this model depends not only on the hopping parameter  $\gamma$  but also on the Coulomb parameter  $U$ .

Both parameters are studied under different filled of the bands, i.e. changing the number of density of electrons on each orbital of the unit cell.

3. Finally, in Chapter 4 a tight-binding model is performed with an electric field. In this case, no study of different values of  $\gamma$  is done, but a transition from metal to an insulator material is reproduced depending on the values of the intensity of the electric field. In this chapter non first-principles neither second-principles codes have been needed, but an analytic formula accomplished.



# Chapter 2

## Tight-binding model

Tight-binding model is a theory developed by Bloch [3] in 1928, and possibly was the first theory that described the behavior of electrons in a crystal. The term "tight-binding" refers to highly localized atomic states, whereas it has taken different meanings [2.3]. There are some cases where tight-binding model has relevant role in electronic structure:

1. Of all the methods, perhaps tight-binding model provides the simplest understanding of the fundamental features of electronic bands.
2. Empirical tight-binding methods can provide accurate, useful descriptions of electronic bands and total energies. In this approach, one assumes a form for the hamiltonian and overlap matrix elements without specifying anything of the orbitals except their symmetry.
3. Local orbitals can be used as a basis to carry out a full self-consistent solution of independent-particle equations.

So with a simple tight-binding method we are able to study electronic bands, total energies and density of states for any system. In order to accomplish this objective it is necessary to solve the time-independent Schrödinger equation

$$\hat{H}\psi_{j\vec{k}}(\vec{r}) = \epsilon_j(\vec{k})\psi_{j\vec{k}}(\vec{r}), \quad (2.1)$$

where  $j$  is a discrete index that labels the different bands and  $\vec{k}$  is a vector of the reciprocal lattice in the first Brillouin zone and both characterizes the wavefunction  $\psi_{j\vec{k}}(\vec{r})$ .

Therefore, it is necessary to define the characteristics of the wavefunction  $\psi_{j\vec{k}}(\vec{r})$ . From now on, let us assume that we will deal with crystalline solids, understanding by that a periodic and ordered structure that can be characterized by a periodic, infinite repetition of a given unit cell in the three

dimensions of real space, according to the prescription given by three lattice vectors. In this kind of systems, the Bloch theorem applies: the eigenfunctions  $\psi_{\vec{j}\vec{k}}$  of a Hamiltonian that is periodic can be written as the product of a plane wave times a function with the periodicity of the lattice

$$\psi_{\vec{j}\vec{k}}(\vec{r}) = e^{i\vec{k}\cdot\vec{r}} u_{\vec{j}\vec{k}}(\vec{r}) \quad / \quad u_{\vec{j}\vec{k}}(\vec{r} + \vec{T}) = u_{\vec{j}\vec{k}}(\vec{r}), \quad (2.2)$$

where  $\vec{T}$  is the translation vector which reproduces the periodicity of the lattice.

As  $u_{\vec{j}\vec{k}}(\vec{r})$  is periodic in the lattice, it has to be defined following the Fourier series for periodic functions

$$u_{\vec{j}\vec{k}}(\vec{r}) = \sum_{\vec{g}} c_{\vec{j}\vec{k}\vec{g}} e^{i\vec{g}\cdot\vec{r}}, \quad (2.3)$$

where  $\vec{g}$  are wavevectors of the reciprocal lattice. Replacing the Eq. (2.3) in Eq. (2.2) it is easy to see that

$$\psi_{\vec{j}\vec{k}}(\vec{r}) = \sum_{\vec{g}} c_{\vec{j}\vec{k}\vec{g}} e^{i(\vec{g} + \vec{k})\cdot\vec{r}}. \quad (2.4)$$

As a corollary of this theorem, it sets how the  $\psi_{\vec{j}\vec{k}}$  functions transform under translations given by the translation vector  $\vec{T}$

$$\psi_{\vec{j}\vec{k}}(\vec{r} + \vec{T}) = e^{i\vec{k}\cdot\vec{T}} \psi_{\vec{j}\vec{k}}(\vec{r}). \quad (2.5)$$

## 2.1 The secular equation

Let's us consider a periodic crystal made up of a periodic repetition of atoms of a given unit cell. The atoms in a unit cell are localized at positions  $\vec{r}_{\kappa,i}$ , where  $\vec{r}_{\kappa,i}$  is the position of the  $i = 1, \dots, n_{\kappa}$  atoms of the atomic species  $\kappa$  (see Fig. 2.1a). In the solid, an atom is localized in position  $\vec{R}_I$  where  $I$  runs over all positions of the atoms. This periodic repetition allows to refer the atoms to the equivalent in the unit cell plus a translation vector (see Fig. 2.1b).

We try to obtain the crystal eigenstates of a hamiltonian in a periodic potential using a set of local orbital basis  $\phi_{\alpha}(\vec{r} - \vec{R}_I)$ , each associated with each atom of the unit cell. It is important to highlight that  $\alpha$  might run over all the atomic orbitals for each atom of the unit cell ( $1s, 2s, 2p, 3d, \dots$ ) (see Fig. 2.1c) but in practice we only include in the simulations the atomic orbitals that participate in the description of the states at the energy window of interest. For this purpose, an

assumption of the tight-binding model is done: close to each lattice point, the crystal Hamiltonian  $\hat{H}$  can be approximated by the Hamiltonian of a single atom  $\hat{H}_{at}$ , so Eq.(2.6) is transformed into

$$\hat{H}_{at} \psi_{j\vec{k}}(\vec{r}) = \varepsilon_j(\vec{k}) \psi_{j\vec{k}}(\vec{r}), \quad (2.6)$$

In order to simplify the notation, we will let  $\mu$  denote both  $\alpha$  and the site  $I$ , so that  $\mu$  runs from 1 to  $N_{\text{basis}}$ , where  $N_{\text{basis}}$  is the total number of atomic orbitals retained in the basis set in a unit cell. With this new notation, the atomic orbital can also be written as  $\phi_{\mu}(\vec{r} - \vec{R}_{\mu})$ . Taking into account that the periodic repetition of the unit cell lets us to represent any position of the solid just referring it as the position of the atom in the unit cell translated a vector  $\vec{T}$ , the composite index  $\{\kappa, i, \alpha \rightarrow \mu\}$  allows the entire basis to be specified by  $\phi_{\mu}[\vec{r} - (\vec{\tau}_{\mu} + \vec{T})]$ . The change of notation is clarified in Fig. 2.1d. The same atomic orbital  $\phi_{\mu}[\vec{r} - (\vec{\tau}_{\mu} + \vec{T})]$  is defined for every atom of the same type in the periodically repeated material and is localized on it but very small a few lattice spacing away. Since the eigenfunctions must comply with the Bloch theorem, it is sensible to define a basis set that comply also with the Bloch theorem. For a given  $\vec{k}$ -point in the first Brillouin zone, it is defined

$$\phi_{\mu\vec{k}}(\vec{r}) = A_{\mu\vec{k}} \sum_{\vec{T}} e^{i\vec{k}\cdot\vec{T}} \phi_{\mu}(\vec{r} - \vec{\tau}_{\mu} - \vec{T}), \quad (2.7)$$

where  $\vec{\tau}_{\mu}$  is the position of the atom within the unit cell to which orbital  $\phi_{\mu}$  belongs, and  $A_{\mu\vec{k}}$  is a normalization factor which is demonstrated to be equal to  $\frac{1}{\sqrt{N}}$  on appendix A.2.

As it is known, a good approximation of the Bloch eigenfunctions is provided by a linear combination of atomic orbitals so

$$\psi_{j\vec{k}}(\vec{r}) \approx \Phi_{\mu\vec{k}}(\vec{r}) = \sum_{\mu} c_{j\mu}(\vec{k}) \phi_{\mu\vec{k}}(\vec{r}). \quad (2.8)$$

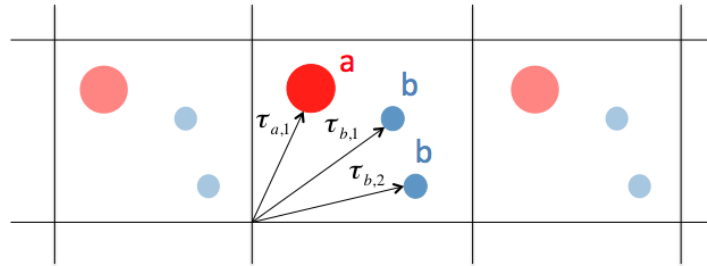
Due to this expansion, in many textbooks the tight-binding approach is known as the linear combination of atomic orbitals (LCAO) approach. So the problem is now to solve the coefficients of expansion  $c_{j\mu}(\vec{k})$  and the energies  $\varepsilon_j(\vec{k})$ .

Replacing the expansion of the eigenfunction in the one-particle Schrödinger equation, it arrives to

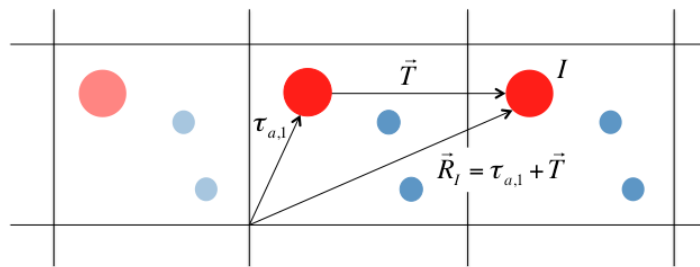
$$\sum_{\mu} c_{j\mu}(\vec{k}) \hat{H} \phi_{\mu\vec{k}}(\vec{r}) = \varepsilon_j(\vec{k}) \sum_{\mu} c_{j\mu}(\vec{k}) \phi_{\mu\vec{k}}(\vec{r}). \quad (2.9)$$

Multiplying at the left by  $\phi_{\mu\vec{k}}^*(\vec{r})$  and integrating all over the space

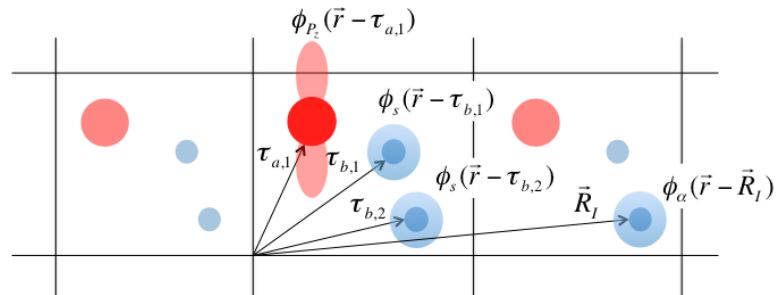
$$\sum_{\mu} c_{j\mu}(\vec{k}) \int_{\text{allspace}} \phi_{\mu\vec{k}}^*(\vec{r}) \hat{H} \phi_{\mu\vec{k}}(\vec{r}) d\vec{r} = \varepsilon_j(\vec{k}) \sum_{\mu} c_{j\mu}(\vec{k}) \int_{\text{allspace}} \phi_{\mu\vec{k}}^*(\vec{r}) \phi_{\mu\vec{k}}(\vec{r}) d\vec{r}, \quad (2.10)$$



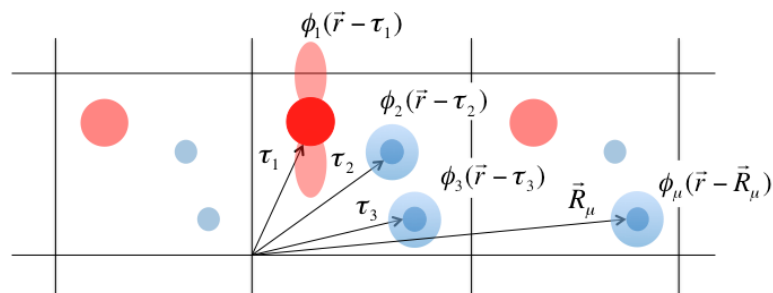
(a) Nomenclature to refer to the position of the atoms in the unit cell.



(b) Nomenclature to refer to the position any atom in the solid.



(c) Nomenclature to refer to the atomic orbitals of any atom.



(d) Nomenclature with composite index.

Fig. 2.1 Nomenclature to refer to the position of the atoms in a unit cell (a), in any position of the crystal (b), or the orbitals of any atom in the solid (c) and with the composite index which allows the entire basis to be referred with only one index (d). The example is done for 2 types of atoms called "a" and "b", with one atom of type "a" and two of type "b", supposing only one orbital per atom.

This expression can be rewritten as

$$\sum_{\mu} c_{j\mu}(\vec{k}) H_{v,\mu}(\vec{k}) = \varepsilon_j(\vec{k}) \sum_{\mu} c_{j\mu}(\vec{k}) S_{v,\mu}(\vec{k}). \quad (2.11)$$

Transposing all the terms to the left hand side in Eq. (2.11),

$$\sum_{\mu} \left( H_{v,\mu}(\vec{k}) - \varepsilon_j(\vec{k}) S_{v,\mu}(\vec{k}) \right) c_{j\mu}(\vec{k}) = 0. \quad (2.12)$$

Where  $H_{v,\mu}$  are the so called hamiltonian matrix elements and  $S_{v,\mu}$  are the overlap matrix elements in a basis of  $\vec{k}$ -dependent Bloch functions. This equation corresponds to Eq. (14.7) of Ref. [12] and it is know as the secular equation.

In the next section it is specified how to obtain the hamiltonian and overlap matrix.

## 2.2 Hamiltonian and overlap matrix elements

### 2.2.1 Hamiltonian matrix elements

The matrix elements of the hamiltonian with basis functions  $\phi_{\mu\vec{k}}(\vec{r})$  and  $\phi_{v\vec{k}'}(\vec{r})$  are given by

$$\begin{aligned} \langle \phi_{\mu\vec{k}}(\vec{r}) | H | \phi_{v\vec{k}'}(\vec{r}) \rangle &= A_{\mu\vec{k}}^* \sum_{\vec{T}} e^{-i\vec{k}\cdot\vec{T}} \int_{\text{all space}} d\vec{r} \phi_{\mu}^*(\vec{r} - \vec{\tau}_{\mu} - \vec{T}) H \left( A_{v\vec{k}'} \sum_{\vec{T}'} e^{i\vec{k}'\cdot\vec{T}'} \phi_v(\vec{r} - \vec{\tau}_v - \vec{T}') \right) \\ &= A_{\mu\vec{k}}^* A_{v\vec{k}'} \sum_{\vec{T}} \left( \sum_{\vec{T}'} e^{i(\vec{k}'\cdot\vec{T}' - \vec{k}\cdot\vec{T})} \int_{\text{all space}} d\vec{r} \phi_{\mu}^*(\vec{r} - \vec{\tau}_{\mu} - \vec{T}) H \phi_v(\vec{r} - \vec{\tau}_v - \vec{T}') \right) \end{aligned} \quad (2.13)$$

In the sum in brackets, the translation vector  $\vec{T}$  is fixed. We can therefore make the following change of variables in the integral  $\vec{r}' = \vec{r} - \vec{T}$ ,

$$\begin{aligned} \langle \phi_{\mu\vec{k}}(\vec{r}) | H | \phi_{v\vec{k}'}(\vec{r}) \rangle &= A_{\mu\vec{k}}^* A_{v\vec{k}'} \sum_{\vec{T}} \left( \sum_{\vec{T}'} e^{i(\vec{k}'\cdot\vec{T}' - \vec{k}\cdot\vec{T})} \int_{\text{all space}} d\vec{r}' \phi_{\mu}^*(\vec{r}' + \vec{T} - \vec{\tau}_{\mu} - \vec{T}) H \phi_v(\vec{r}' + \vec{T} - \vec{\tau}_v - \vec{T}') \right) \\ &= A_{\mu\vec{k}}^* A_{v\vec{k}'} \sum_{\vec{T}} \left( \sum_{\vec{T}'} e^{i(\vec{k}'\cdot\vec{T}' - \vec{k}\cdot\vec{T})} \int_{\text{all space}} d\vec{r}' \phi_{\mu}^*(\vec{r}' - \vec{\tau}_{\mu}) H \phi_v \left[ \vec{r}' - \vec{\tau}_v - (\vec{T}' - \vec{T}) \right] \right) \end{aligned} \quad (2.14)$$

Now, making the change in variables  $\vec{T}' - \vec{T} = \vec{T}''$ ,

$$\begin{aligned}
\langle \phi_{\mu\vec{k}}(\vec{r}) | H | \phi_{\nu\vec{k}'}(\vec{r}) \rangle &= A_{\mu\vec{k}}^* A_{\nu\vec{k}'} \sum_{\vec{T}} \left( \sum_{\vec{T}''} e^{i(\vec{k}' \cdot (\vec{T}'' + \vec{T}) - \vec{k} \cdot \vec{T})} \int_{\text{all space}} d\vec{r}' \phi_{\mu}^*(\vec{r}' - \vec{\tau}_{\mu}) H \phi_{\nu}(\vec{r}' - \vec{\tau}_{\nu} - \vec{T}'') \right) \\
&= A_{\mu\vec{k}}^* A_{\nu\vec{k}'} \left[ \sum_{\vec{T}} e^{i(\vec{k}' - \vec{k}) \cdot \vec{T}} \right] \left( \sum_{\vec{T}''} e^{i\vec{k}'' \cdot \vec{T}''} \int_{\text{all space}} d\vec{r}' \phi_{\mu}^*(\vec{r}' - \vec{\tau}_{\mu}) H \phi_{\nu}(\vec{r}' - \vec{\tau}_{\nu} - \vec{T}'') \right) \\
&= N \delta_{\vec{k}, \vec{k}'} A_{\mu\vec{k}}^* A_{\nu\vec{k}'} \left( \sum_{\vec{T}''} e^{i\vec{k}'' \cdot \vec{T}''} \int_{\text{all space}} d\vec{r}' \phi_{\mu}^*(\vec{r}' - \vec{\tau}_{\mu}) H \phi_{\nu}(\vec{r}' - \vec{\tau}_{\nu} - \vec{T}'') \right),
\end{aligned} \tag{2.15}$$

where we have used Eq. (2.16) [see Ref. [2], Eq. (F.4)]

$$\sum_{\vec{T}} e^{i\vec{k} \cdot \vec{T}} = N \delta_{\vec{k}, \vec{0}}, \tag{2.16}$$

where  $\vec{T}$  runs through the  $N$  sites of the Bravais lattice in Eq. (2.16).

Now, denoting the matrix element of the hamiltonian of a orbital  $\mu$  in the unit cell at the origin and an orbital  $\nu$  in the cell labeled by translation vector  $\vec{T}''$ ,

$$H_{\mu, \nu}(\vec{T}'') = \int_{\text{all space}} d\vec{r}' \phi_{\mu}^*(\vec{r}' - \vec{\tau}_{\mu}) H \phi_{\nu}(\vec{r}' - \vec{\tau}_{\nu} - \vec{T}''), \tag{2.17}$$

Eq. (2.15) transforms into

$$\langle \phi_{\mu}(\vec{k}) | H | \phi_{\nu}(\vec{k}') \rangle = N \delta_{\vec{k}, \vec{k}'} A_{\mu\vec{k}}^* A_{\nu\vec{k}'} \left( \sum_{\vec{T}''} e^{i\vec{k}'' \cdot \vec{T}''} H_{\mu, \nu}(\vec{T}'') \right) \tag{2.18}$$

Finally, assuming that the normalization factors of the Bloch orbitals are  $\frac{1}{\sqrt{N}}$ , we finally arrive to

$$H_{\mu, \nu}(\vec{k}) = \langle \phi_{\mu}(\vec{k}) | H | \phi_{\nu}(\vec{k}) \rangle = \sum_{\vec{T}} e^{i\vec{k} \cdot \vec{T}} H_{\mu, \nu}(\vec{T}), \tag{2.19}$$

that corresponds to Eq. (14.4) of Ref. [12].

## 2.2.2 Overlap matrix elements

By analogy, the matrix elements of the overlap matrix between Bloch basis orbitals  $\phi_{\mu}(\vec{k})$  and  $\phi_{\nu}(\vec{k}')$  are also diagonal in  $\vec{k}$  and equals

$$S_{\mu,\nu}(\vec{k}) = \langle \phi_{\mu}(\vec{k}) | \phi_{\nu}(\vec{k}) \rangle = \sum_{\vec{T}} e^{i\vec{k}\cdot\vec{T}} S_{\mu,\nu}(\vec{T}). \quad (2.20)$$

This corresponds with Eq. (14.5) of Ref. [12].

## 2.3 Tight-binding bands

As an example of the calculations which can be carried out with the analysis presented along this chapter, the most simple lattices 1D, that represents a linear chain; 2D, that represents a square lattice; and 3D, that represents a cubic crystal, have been studied. For them, it is supposed to have only one  $s$  orbital per atom in the unit cell each on site  $I$  in Bravais lattice, with no overlaps between them, with only one electron per atom, identical atoms in each node and interaction only with first neighbors.

All of this simplifications means that we will obtain only one band corresponding to  $s$  band half-occupied, with the Fermi energy  $E_F$  at the middle of the bands. The simplification of taking into account only the first neighbors lead us to have non-zero hamiltonian matrix elements  $\langle I | \hat{H} | I' \rangle \equiv -\gamma$  only if  $I$  and  $I'$  are nearest neighbors. Moreover, it has been supposed that the on-site term can be chosen to be zero,  $\langle 0 | \hat{H} | 0 \rangle = 0$ . The fact of consider zero overlapping between orbitals make the term  $S_{\mu,\nu}(\vec{k})$  to be zero except when having  $\mu$  equal to  $\nu$ , that is  $S_{\nu,\nu}(\vec{k}) = 1$ . With this conditions transform Eq. (2.12) into

$$\varepsilon(\vec{k}) = H_{\nu,\mu}(\vec{k}) = -\gamma \sum_{\vec{T}} e^{i\vec{k}\cdot\vec{T}} \quad (2.21)$$

The only difference between the simulated 1D, 2D and 3D cases is in the number of addends in Eq. (2.21). For the most complex one, the 3D case, this equation is equal to

$$\varepsilon(\vec{k}) = -2\gamma[\cos(\vec{k}_x a) + \cos(\vec{k}_y a) + \cos(\vec{k}_z a)] \quad (2.22)$$

where  $a$  is the parameter of the lattice.

The bands obtained for each lattice are illustrated in Fig. 2.2.

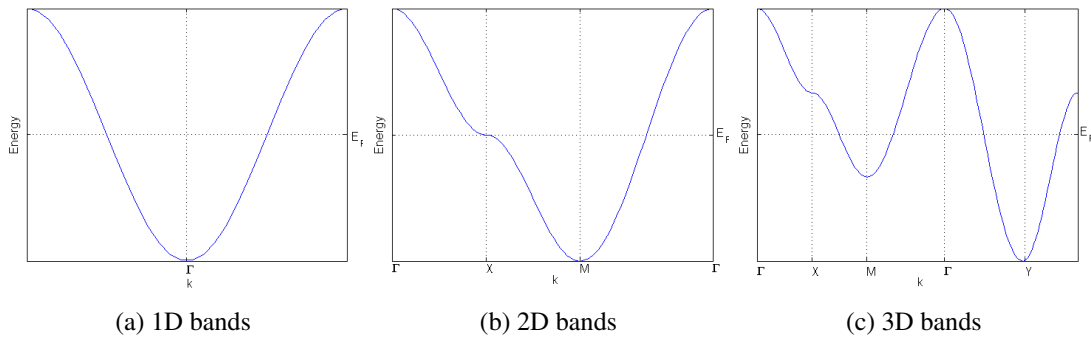


Fig. 2.2 Tight-binding bands in one (a), two (b) and three (c) dimensional lattice with only an  $s$  state on each site and first neighbors interactions. The figures shows the bands with  $\vec{k}$  along the lines between the high-symmetry points.

These simple examples leads to useful insights. In particular, as it can be observed in Fig. 2.2, the bands are symmetric about  $\varepsilon(\vec{k}) = 0$ . In order to clarify this symmetry in Fig. 2.3 the bands in the 2D case are represented along both directions  $\vec{k}_x$  and  $\vec{k}_y$  against the energy of each state.

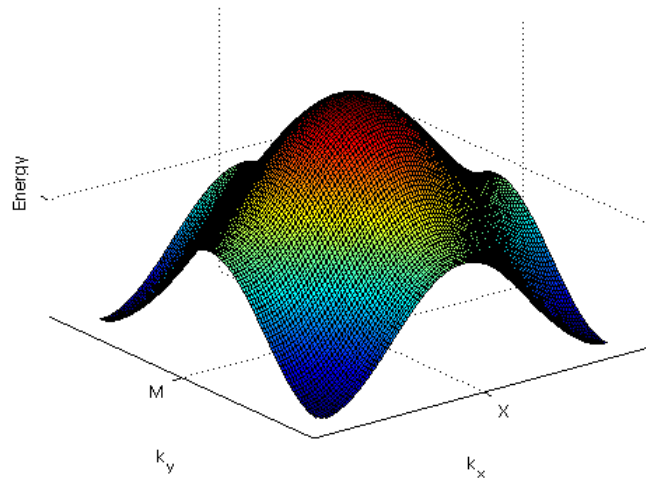


Fig. 2.3 Three dimensional tight-binding band in a square lattice with only a  $s$  state on each site and first neighbors interactions.

The same arguments could be applied to the linear chain and the crystal case. As it can be derived from Eq. (2.22), the bands for the one dimensional problem is a simple cosine bands. The width of the bands can be found analytically through Eq. (2.22) obtaining a value of  $4\gamma$ .

This parameter  $\gamma$  is the main parameter that characterizes the bands. A larger value of  $\gamma$  is associated with wider bands, larger hopping and then, metallic states. Opposite situation is found for smaller values of  $\gamma$  which means flatter bands and shorter hopping, typical of insulating states.

The density of states (dos) for each case are illustrated in Fig. 2.4.

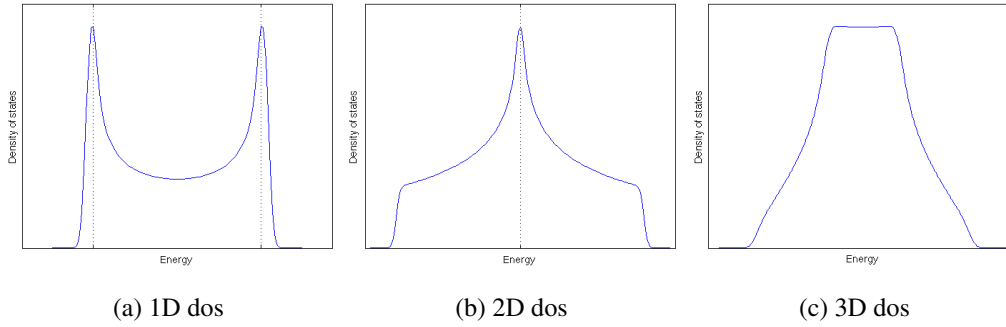


Fig. 2.4 Tight-binding bands in one (a), two (b) and three (c) dimensional lattice with only an  $s$  state on each site and first neighbors interactions. The figures show the bands with  $\vec{k}$  along the lines between the high-symmetry points.

These figures highlight the fact that the density of states shows a peak in the energies corresponding to regions of flat bands. Because of that, in Fig. 2.4a appear two peaks corresponding to the maximum and minimum energies, and in Fig. 2.4b only appear one, corresponding to the high-symmetry point  $M$ . This point has a special property. Since the bands on it curve upward and downward in different directions, the density of states have a mathematical logarithmic divergence at  $\epsilon(\vec{k}) = 0$ , although it has been drawn with a maximum. This behavior is because in this simple case we are only considering first neighbors interactions but for second neighbors interactions, the symmetry of the bands is broken and the divergence disappears (Ref. [12]). For the first case, shown in Fig. (2.4a), it can be seen that in this two maximums the DOS function decreases out of the limits of the bands (out of  $\vec{k} = -\frac{\pi}{a}$  and  $\vec{k} = \frac{\pi}{a}$ ). This is owing to the mathematical way of representing the density of states but obviously there are no states out of the limits of  $\vec{k}$ .

Later on, it has been discussed some examples where two atoms per unit cell are needed. In Fig. 2.5 is shown the electronic  $s$ -band for a 1D lattice. As it can be observed, the band is folding around Bragg planes in  $k = -\frac{\pi}{a}$  and  $k = \frac{\pi}{a}$ , so it means the double the cell in real space is the half the cell in reciprocal space, as is widely known.

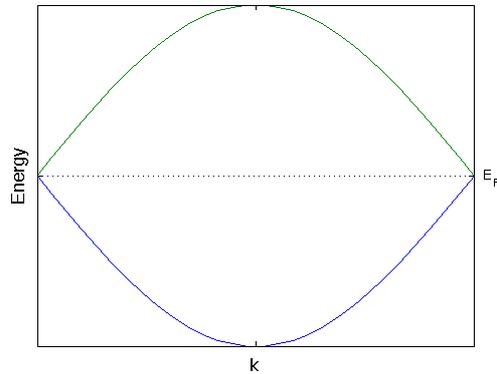


Fig. 2.5 One dimensional tight-binding band for a chain lattice with only a  $s$  state on each site and first neighbors interactions and two atoms per unit cell.

## 2.4 Conclusions

In this introductory chapter the tight-binding model is studied. This simple model reproduces the structure of the electronic bands of systems only taking into consideration the  $\gamma$  parameter which is related with the kinetic energy of the electrons in a unit cell. It has been shown that for a larger values of  $\gamma$ , metallic states are reproduced, while for shorter values of  $\gamma$  the band width is reduced so an insulating state is approached.

This model is very useful in many cases but combined with some other models it reproduces a wide variety of solids giving better results.

# Chapter 3

## The Hubbard model

In the Chapter 2 a simple tight-binding model was studied. This model doesn't take into account the spin of the electrons. In this chapter as the spin of the electrons is introduced, the hamiltonian of the system is the one behind the Hubbard model.

The Hubbard model was independently conceived by Martin Gutzwiller [6], Junjiro Kanamori [10] and John Hubbard [9] in 1963. The main motivation was the need for a way to tackle the behavior of correlated electrons in solids. Initially, the model was introduced to provide an explanation for the itinerant ferromagnetism of transition metals but its relevance go far beyond that original context.

Technically, the Hubbard model is an extension of the tight-binding model where, as explained in Chapter 2, the electrons can hop between lattice sites with a probability given by the hopping  $\gamma$ . The movement of these electrons is characterized by their kinetic energy, represented by hopping  $\gamma$ . Hubbard's hamiltonian features an additional term, introducing an energy amount  $U$  for each pair of electrons occupying the same lattice site representing Coulomb repulsion. Hubbard found the model to be the simplest that produces both a metallic and an insulating state, depending on the value of  $U$ . For one electron per lattice site, the Mott transition is reproduced. This is a type of metal-insulator transition that could not be understood in terms of conventional band theory and the first one discussed in this thesis.

The simplicity of the Hubbard model when written down is deceptive: an exact solution has so far obtained for the one-dimensional case [4]. Because of that, in this chapter it is only discussed that one-dimensional case.

### 3.1 The Hubbard Hamiltonian

Let's consider a periodic lattice of atoms in a solid whose positions are fixed and on which the electrons move. For the sake of simplicity, it is assumed that the atoms do have only an  $s$ -symmetry state on each site of the Bravais lattice. The Hubbard Hamiltonian is formed by two terms. The first term is the one described by the tight-binding model and is related with the hopping of the electrons from one site of the lattice to the neighbors. Following the notation of Chapter 2, the hopping is referred to as  $\gamma$ . As  $\gamma$  is determined by the overlap of the wavefunctions of a pair of atoms and they decrease exponentially, it has been only considered the hopping between the first neighbors.

As Pauli's Principle indicates and in a model with only one state per site, the maximum number of electrons per atom is two and they must have different spin. The electrons with opposite spins of a given state would repeal each other via electrostatic forces. This forces can be quantified by a Coulomb parameter usually referred to as  $U$ , defined as the energy ... to put two electrons opposite spin in the same atom site. The model doesn't consider interaction between electrons on different sites.

Let's now formalize the construction. Written in second quantization notation, the Hubbard hamiltonian is given by

$$H = -\gamma \sum_{\langle l,m \rangle, \sigma} c_{l\sigma}^\dagger c_{m\sigma} + U \sum_l n_{l\uparrow} n_{l\downarrow} \quad (3.1)$$

The first term is the so called hopping integral and it represents the kinetic energy of an electron of spin  $\sigma$  hopping between atoms on site  $l$  and  $m$ . So  $c_{l,\sigma}^\dagger$  is the creation term and represents the creation of an electron on site  $l$  coming from  $m$  represented by the annihilation term,  $c_{m,\sigma}$ , both of them with spin  $\sigma$ . The notation of  $\langle l,m \rangle$  remarks that hopping is only allowed on adjacent sites. This hopping will be determined by the overlap of the two wavefunctions. Since the wavefunctions die off exponentially, the simplification of consider only the first neighbors is reasonable. The second term is the interaction energy which goes through all sites and adds an energy  $U$  if it finds that the site is doubly occupied. So the term  $n_{l\uparrow}$  refers to the number of electrons with spin up on site  $l$ , and analogously,  $n_{l\downarrow}$  refers to the number of electrons with spin down on the same site  $l$ . As it can be deduced, both density of electrons will run from 0 to 1.

Whereas the hopping matrix elements can usually be determined accurately in the framework of density-functional theory, the effective interaction parameter  $U$  is much more difficult to estimate and is perhaps best fixed by comparing theoretical predictions to experimental results.

Now a more difficult hamiltonian should be studied. The goal of this chapter is to find what is the state that minimizes the energy given by the hamiltonian of the Eq. (3.1). That state is going to

be characterized by three parameters: the hopping parameter  $\gamma$ , the Hubbard- $U$  and the occupation  $n_{I\uparrow}$  and  $n_{I\downarrow}$ , which is related with the doping with impurities in an experimental set up.

### Some hand-waving considerations

Let's see some hand-waving considerations about each parameter:

1. First of all, as shown in Chapter 2, the larger the  $\gamma$ , the larger the hopping, the broader the band width. In other words, a metallic phase is favored.
2. Secondly, the  $U$  penalize the occupation of a site with electrons of different spin. If a given atom is already occupied with a given density of electrons of a given spin, the electrons with different spin will feel a repulsion to hop there. Therefore the  $U$  inhibits somehow the hopping and favors localized states.
3. Finally, the effect of having a repulsion strongly depends on the occupation. If the occupation is lower than half-filled limit, the system could accommodate the electrons in a way that results in a metallic state. However, if the occupation is greater than the half filled limit, each site is going to be occupied by density of electrons of both spins, so the final configuration is governed by the later two parameters.

In conclusion, not only the value of  $U$  is important but its relation with the value of  $\gamma$  would determine the equilibrium of the system. Moreover, these two parameters become more significant depending on the occupation. Half-filling limit seems to be important because a transition from metal to insulator could emerge. In principle, when  $U \ll \gamma$  a metallic state should be obtained whereas when  $U \gg \gamma$  it is expected to have an insulator material as the system approaches the atomic limit.

Along this chapter, a ferromagnetic and antiferromagnetic linear chains are studied varying the initial conditions trying many values of  $U/\gamma$ , not only for the half-filled limit but for some other occupations. Further on it is demonstrated that not all systems are stable under some specific conditions imposed, but some configurations usually have less energy so the system tends to them.

## 3.2 Shape of the electronic bands and density of states

The first point to take into account is that now the spins up and down could be not degenerated. This will be reflected both in the electronic bands and density of states. In this section, some aspects are clarified for a good interpretation of this bands in the examples made in this chapter.

In the quest for the ground state of the Hubbard hamiltonian described in Eq. (3.1), three different physical scenarios are considered: a diamagnetic, a ferromagnetic and an antiferromagnetic configurations.

### Diamagnetic configuration

It occurs when the occupation for the up and down state is the same on every site, (Fig. 3.4a). Due to this symmetry, both the band structure and DOS must be the same for both spin components, (Fig. 3.1b, Fig. 3.1c). Their shape is the same as in the tight-binding model (Fig. 2.2a, Fig. 2.4a), but shifted towards more plus energy, due to the Coulomb term  $Un_{i\uparrow}n_{i\downarrow}$ .

### Ferromagnetic configuration

It occurs when the occupation for one of the spin channel (*majority spin*) is larger than the other (*minority spin*). The majority spin channel is the same for all the lattice sites, (Fig. 3.1d) up, which means all the lattice sites are equivalent. Clearly, the introduction of an  $U$  is going to add a term in the energy expression. For the *majority spin*, the on-site hamiltonian matrix elements in real space, related with the center of mass of the band, changes from  $\alpha$  (with  $U = 0$ ) to  $\alpha - 2U\delta n$  as is demonstrated on Appendix B (Eq. B.32), calling  $D_{aa}^\uparrow = \delta n$ . The same downwards shift is observed for all the lattice sites. Therefore, the corresponding hamiltonian in reciprocal space for a given  $k$ -point in a linear chain and for the spin up channel, following Appendix B, Eq. B.39, is

$$h_{ab}^\uparrow(k) = \begin{pmatrix} \alpha - 2U\delta n & \gamma(1 + e^{-i2ka}) \\ \gamma(1 + e^{i2ka}) & \alpha - 2U\delta n \end{pmatrix}.$$

In order to have non-trivial solutions, the determinant  $|h_{ab}^\uparrow(k) - E_n^\uparrow(k)|$  must be equal to zero, and this happens when

$$E_n^\uparrow(k) = (\alpha - 2U\delta n) \pm 2\gamma\cos(ka) \quad (3.2)$$

For the *minority spin* the same reasoning holds, with the exception that the center of mass of the bands moves upwards in energy a quantity  $\alpha + 2U\delta n$  as is demonstrated on Appendix B (Eq. B.40). Then, the energy of the bands for down spin is given by

$$E_n^\downarrow(k) = (\alpha + 2U\delta n) \pm 2\gamma\cos(ka) \quad (3.3)$$

in coincidence with the bands drawn in Fig. 3.1e and DOS plotted in Fig. 3.1f.

Looking at Eq. (3.5) and Eq. (3.3) some conclusions can be extracted:

1. Both spin channel bands moves a rigid shift in relation with the diamagnetic configuration. In other words, the bands have the same shape but are centered downwards, for *majority spin*, and upwards, for *minority spin*, the same absolute quantity  $2U\delta n$ . An sketch of the energy levels is drawn in Fig. 3.1d down.
2. As this shift only depends on the value of  $U$ , bands for each spin channel the relative move between bands is equal to  $4U\delta n$ .
3. The width of the bands is independent of the value of  $U$  but equal to the width of the bands in a simply tight-binding model. That is, the width is  $4\gamma$  and is the same for both spin channels.
4. Paying attention to the picture of Fig. 3.1d down, as the energy of the *majority spin* of one lattice site is the same than the energy of the *majority spin* of its first neighbors, a metallic material is expected provided the occupation  $n_l$  is less than 1. Obviously, the same occurs for *minority spin*.

### Antiferromagnetic configuration

It is produced when the occupation for the *majority spin* is the same than the occupation for the *minority spin* having not equivalent lattice sites, but opposite situations as in (Fig. 3.1g) up. Proceeding the same way as in ferromagnetic configuration, the corresponding hamiltonian in reciprocal space for a given  $k$ -point in a linear chain for the spin up channel is

$$h_{ab}^{\uparrow}(k) = \begin{pmatrix} \alpha + 2U\delta n & \gamma(1 + e^{-i2ka}) \\ \gamma(1 + e^{i2ka}) & \alpha - 2U\delta n \end{pmatrix},$$

where the terms are taken from Eq. B.41 of Appendix B. Solving the same determinant than in the previous case, the energies obtained are given by the expression

$$E_n^{\uparrow}(k) = \alpha \pm 2\gamma \sqrt{\cos^2(ka) + \frac{U^2\delta n^2}{\gamma^2}} \quad (3.4)$$

For the *minority spin* the same steps are followed, but the on-site terms of the hamiltonian in real space changes to

$$h_{ab}^{\downarrow}(k) = \begin{pmatrix} \alpha - 2U\delta n & \gamma(1 + e^{-i2ka}) \\ \gamma(1 + e^{i2ka}) & \alpha + 2U\delta n \end{pmatrix}$$

according to Eq. B.42 of Appendix B. Despite having different signs, the symmetry of the hamiltonian makes the solution to be the same than for spin up. So

$$E_n^\downarrow(k) = \alpha \pm 2\gamma \sqrt{\cos^2(ka) + \frac{U^2 \delta n^2}{\gamma^2}} \quad (3.5)$$

is also the energy of the band for the *minority spin*.

Some important characteristics come to light:

1. The energy for the bands of spin up is equal to the bands obtained for spin down. That's it, bands are degenerated.
2. There is no a rigid shift. Instead, another shape of the bands is obtained.
3. If the energy is evaluated in the Bragg planes, meaning  $k = \frac{-\pi}{2a}$  and  $k = \frac{\pi}{2a}$ , for both spins is  $E_n^\sigma = \alpha \pm \frac{U\delta n}{\gamma}$ , so a gap of energy  $2\frac{U\delta n}{\gamma}$  is opened in the limits of first Brillouin zone, which is in agreement with Fig. 3.1h and Fig. 3.1i.
4. The width of the bands depends on  $U$ , and for the upper bands, is of the form:

$$w = 2\gamma \sqrt{1 + \frac{U^2 \delta n^2}{\gamma^2}} - 2U\delta n \quad (3.6)$$

For the lower bands, this expression only changes its sign, but the absolute value of the width is obviously the same.

In the view of the fact that the width is proportional to  $U$ , one could think that the higher  $U$  the wider the bands, but is exactly the opposite because the first term of Eq. (3.6) increases, for low values of  $U$ , slower than the second term; and for high values of  $U$ , at the same rhythm. Even more the term  $2U\delta n$  is an asymptote of the function  $2\gamma \sqrt{1 + \frac{U^2 \delta n^2}{\gamma^2}}$ . In Fig. 3.2 a graphical representation of both terms is done. So for a given  $U$ , the band width is exactly the difference between the two drawn lines.

This conclusion is very important as is in agreement with the fact that the higher the repulsion term, the flatter the bands, the more localized the electrons on its sites and, as a result, the more insulator material.

5. Paying attention to the picture of Fig. 3.1g down, now the energy of the *majority spin* of one lattice site is less than the energy of the *majority spin* of its first neighbors so, depending on this penalty in energy, an insulator material is expected independently of the occupation  $n_l$ .

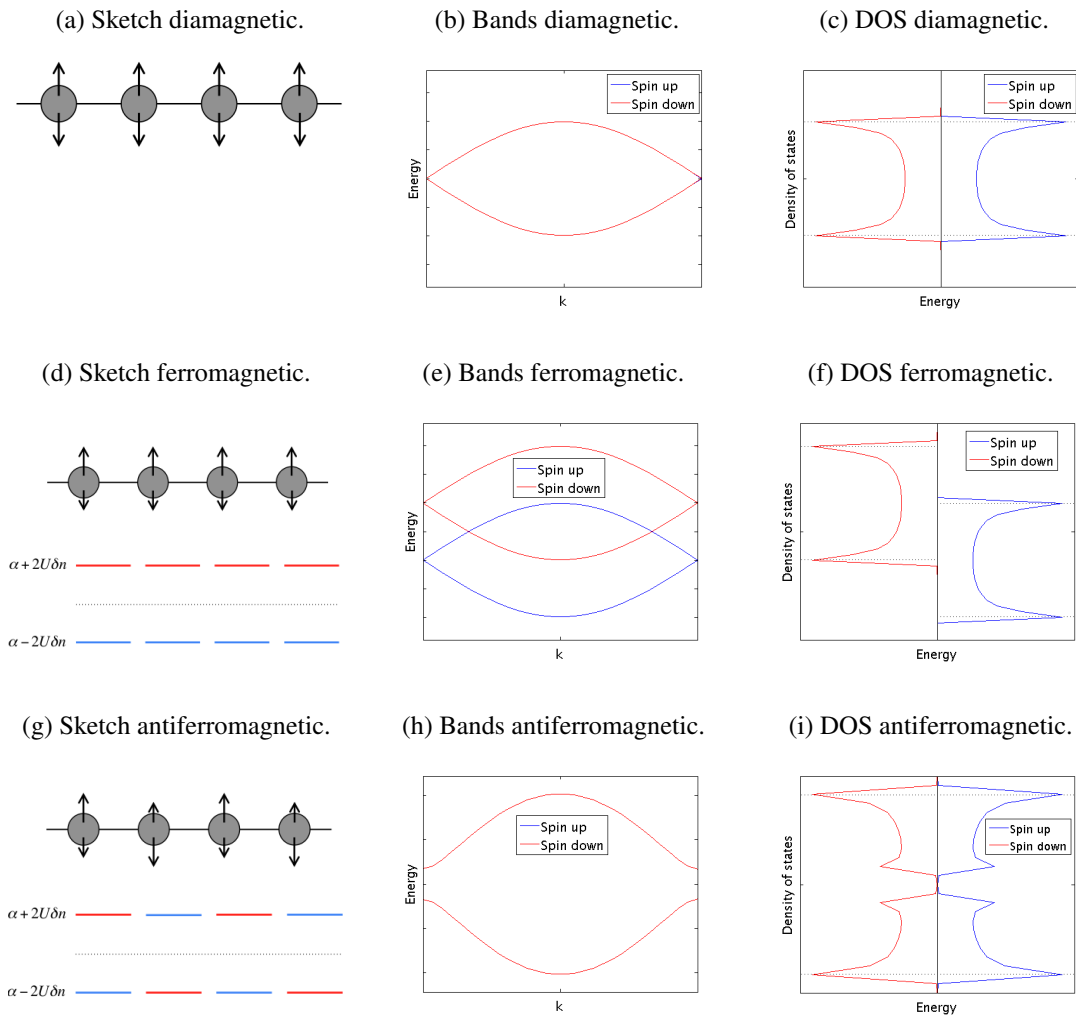


Fig. 3.1 Plots of the sketch, bands and DOS for each configuration considered. The first row belongs to a diamagnetic material, second row to a ferromagnetic material and third row to an antiferromagnetic material.

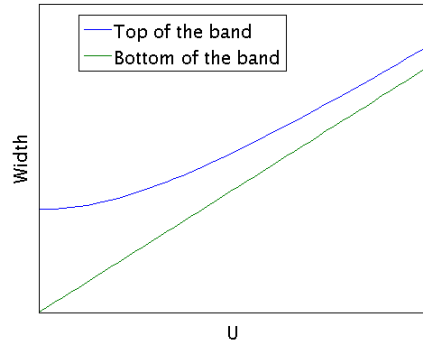


Fig. 3.2 Width of an  $s$  state for an antiferromagnetic linear chain. Blue line corresponds to the first term of Eq. (3.6), and green line with the second term of the same equation. The width is the difference between the value given by the blue line minus the one of the green line for a given  $U$ .

### 3.3 Ferromagnetic chain

In this section results obtained from the simulation of a ferromagnetic linear chain under different conditions is summarized. As the importance of the parameters  $U$  and  $\gamma$  falls to its relation, a fixed value of  $\gamma$  is chosen and is the value of  $U$  which has been changed. In this section, only the half-filling limit is studied.

If a linear chain of equal atoms, only taking into account their  $s$  orbital, with electrons with its spins pointing up is simulated, actually a totally polarized ferromagnetic material is performed. A simply sketch of the simulated chain appears in Fig. 3.3 and represents the half-filled limit because there are just enough electrons to have one in each lattice site.

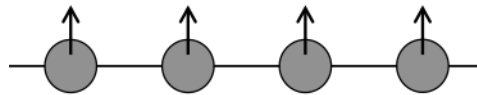


Fig. 3.3 Totally polarized ferromagnetic linear chain for half-filling limit and only a  $1s$  state per each lattice site

At this point some concept explained before has to be remarked. The Hubbard model reproduces a repulsive interaction given by  $U$  if exists electrons of opposite spin in the same site. When a  $1s$  orbital is studied, a maximum of one entire electron with spin up could stay in each atom and the same occurs for a spin down electron. Nevertheless, the range for  $n_{l\sigma}$ , with  $\sigma = \uparrow$  or  $\downarrow$ , is maintained between 0 and 1. A fraction of  $n_{l\sigma}$  could be interpreted as a fraction of electron is occupying the atom. When this occurs, one fraction of electron could jump to its neighbor if the

sum of both fraction of electrons were 1 or less, and no  $U$  will be added due to the fact that it is understood it will complete the rest of the electron until achieve an entire spin.

So for a given starting point of having a 1D ferromagnetic system, now is wanted to know if this system is stable. A hopping  $\gamma = 0.5$  eV and a value of Hubbard- $U$  of 0.1 eV is written down in the input file of the SCALE-UP software. After some convergence steps the result is that the system converges to the one shown in Fig. 3.4a which electronic bands and density of states are drawn in Fig. 3.4b and Fig. 3.4c, respectively. This figures are essentially the same to the ones that appear in Fig. 3.1b and Fig. 3.1c, but where the Fermi energy indicates that the material has each lattice site occupied by  $n_i^\uparrow = 0.5$  and  $n_i^\downarrow = 0.5$ .

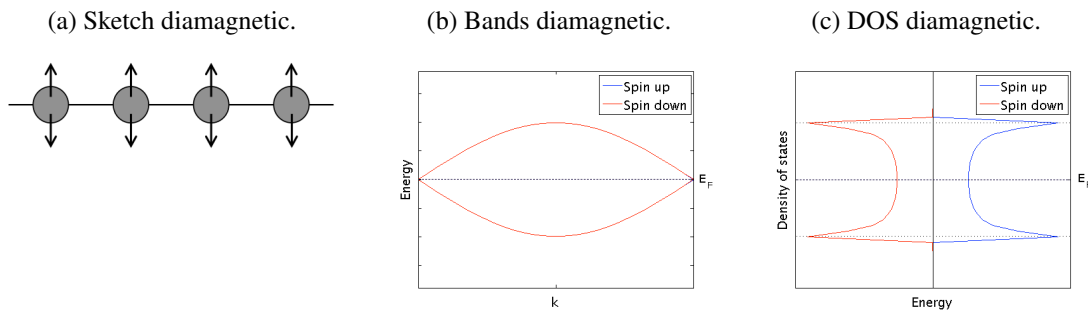


Fig. 3.4 Plots of the sketch, bands and DOS of the most stable system under hopping  $\gamma = 0.5$  eV,  $U = 0.1$  eV and half-filling limit. Dotted line indicates where Fermi energy is localized.

Taking into consideration the concepts explain on the last section, the electrons could jump freely. This means that even though a repulsion is acting between electrons in each atom, it is not enough to overcome the kinetic energy so an antiparallel configuration of spins is favored until half electron has its spin pointing up and half electron has its spin pointing down.

Some important conclusion is derived from this simulation. For a initial ferromagnetic chain under hopping and Hubbard- $U$  parameters equals to 0.5 eV and 0.1 eV respectively, it will end up with a non-magnetic metallic material. So no stable system could be achieved for a ferromagnetic chain under this specific conditions.

Some other values of  $U$  were tried, changing the relation  $U/\gamma$ . To achieve this objective, a value of  $\gamma = 0.5$  remains fixed. On Table 3.1 are summarized different cases simulated.

Case	$U/eV$	$\gamma/eV$	$U/\gamma$	$\Delta E = E - E^0 /eV$	Material
1	0.0	0.5	0.0	-1.27308	Diamagnetic
2	0.1	0.5	0.2	-1.27308	Diamagnetic
2	0.2	0.5	0.4	-1.27324	Antiferromagnetic
2	0.5	0.5	1.0	-1.28258	Antiferromagnetic
3	0.6	0.5	1.2	-1.29934	Antiferromagnetic
5	0.8	0.5	1.6	-1.36559	Antiferromagnetic
6	0.9	0.5	1.8	-1.41342	Antiferromagnetic
7	1.0	0.5	2.0	-1.46910	Antiferromagnetic
10	1.5	0.5	3.0	-1.50000	Ferromagnetic insulator
11	2.0	0.5	4.0	-2.00000	Ferromagnetic insulator
12	3.0	0.5	6.0	-3.00000	Ferromagnetic insulator

Table 3.1 Values of  $U/\gamma$  simulated for a ferromagnetic chain with one electron per lattice site.

So at  $U/\gamma = 0.2$  eV a transition emerges: from a metallic material to an insulator antiferromagnetic material. This transition is the so called Mott transition. This results are partially in agreement with Ref. [11]. On this reference the same study were done and the conclusion is that no Mott transition appears for  $U \neq 0$ .

Paying attention to the last three converged systems of the table, a so called ferromagnetic insulator appears. In this case, the  $U$  (compared with  $\gamma$ ) is larger enough to make the electrons be completely localized that the simulation could not move it to try another configuration less energetic so all the spins remains up making the linear chain be totally polarized. The electronic bands, Fig. 3.5a, and DOS, Fig. 3.5b, for each spin flavor are completely separated and a gap appears. The Fermi energy is located somewhere in the middle of the gap.

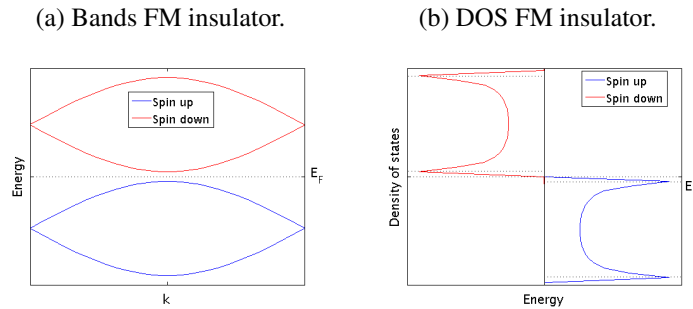


Fig. 3.5 Plots of the sketch, bands and DOS the most stable system under hopping  $\gamma = 0.5$  eV,  $U = 0.1$  eV and half-filling limit. Dotted line indicates where Fermi energy is localized.

With the next example, this transition obtained with  $U/\gamma = 3.0$  eV is clarified.

### 3.4 Antiferromagnetic chain

Not only a ferromagnetic linear chain was studied but a totally polarized antiferromagnetic linear chain also. For this case, each electron with spin up is surrounded by two with spin down and so on. The same occupation cases are studied for this example. In Fig. 3.6 a sketch of the system to simulate is drawn, that serves as first step for the self-consistent cycle.

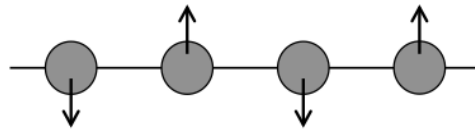


Fig. 3.6 Totally polarized antiferromagnetic linear chain for half-filling limit and only a  $1s$  state per each lattice site.

After running the simulation, the same result as the previous one is obtained: the system will end up in a diamagnetic system (Fig. 3.5a and Fig. 3.5b). Other values tried with this configuration are shown on Table 3.2 where are summarized.

Case	$U/eV$	$\gamma/eV$	$U/\gamma$	$\Delta E = E - E^0/eV$	Material
1	0.0	0.5	0.0	-1.27308	Diamagnetic
2	0.1	0.5	0.2	-1.27308	Diamagnetic
2	0.2	0.5	0.4	-1.27324	Antiferromagnetic
2	0.5	0.5	1.0	-1.28258	Antiferromagnetic
3	0.6	0.5	1.2	-1.29934	Antiferromagnetic
5	0.8	0.5	1.6	-1.36559	Antiferromagnetic
6	0.9	0.5	1.8	-1.41342	Antiferromagnetic
7	1.0	0.5	2.0	-1.46910	Antiferromagnetic
10	1.5	0.5	3.0	-1.82409	Antiferromagnetic
11	2.0	0.5	4.0	-2.24609	Antiferromagnetic
12	3.0	0.5	6.0	-3.16551	Antiferromagnetic

Table 3.2 Values of  $U/\gamma$  simulated for an antiferromagnetic chain.

In Fig. 3.7 values of the energy on Table 3.1 and Table 3.2 are compared. It could be noticed that the energy is the same up to  $U/\gamma = 1$  eV and then decreases faster for an antiferromagnetic

linear chain. This is the reason why there is no transition from antiferromagnetic to a ferromagnetic insulator when a 1D system is simulated: an antiferromagnetic configuration has always less energy so the nature will tend to this state.

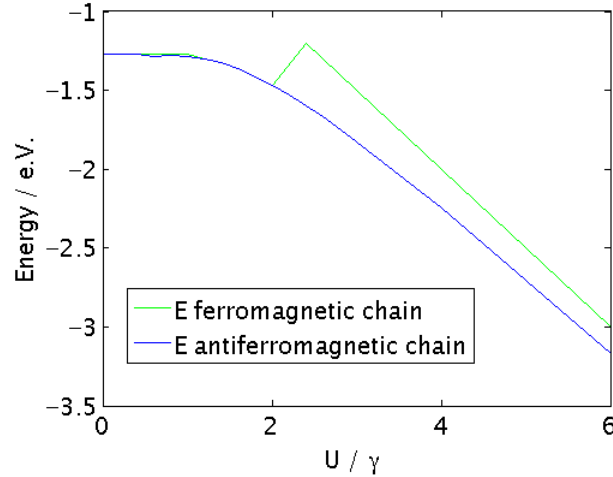


Fig. 3.7 Comparison between the energy of the converged system in a ferromagnetic and antiferromagnetic linear chain simulations for  $n_l^\sigma = 0.5$ .

The conclusion that could be derived from this study is that for half-filling limit, no Mott transition is found for a 1D system. The reason of this result might be explained from the DOS. Density of states of 1D systems, shows a divergence in two  $k$ -points corresponding with flat bands. This divergence disappears for 3D systems, as shown in Chapter 1 (Fig. 2.4c)

### 3.5 Transition diagrams

On the last section a study for two different linear chains in the half-filled limit have been done. If the same study is repeated for some other occupations trying different values of  $U/\gamma$  for each case, a transition phase diagram can be mapped. In order to be able to draw a diagram with the converged systems for simulations with 1D ferro and antiferromagnetic linear chains, energies should be compared for each occupation as was done some lines above. With the comparison of this representations, one can discern which system is more stable. Analogous representations to Fig. 3.7 for many other occupations can be consulted in Appendix C.

In Fig. 3.8 is represented the transition phase diagram when starting with a ferromagnetic linear chain.

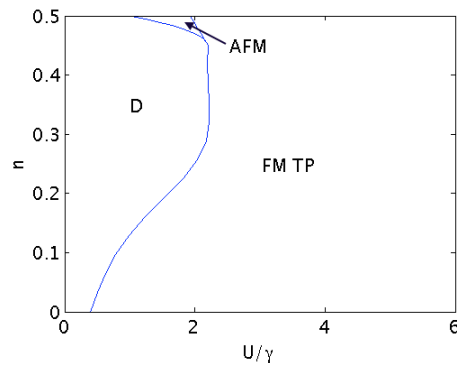


Fig. 3.8 Phase diagram for a simulation started with a totally polarized ferromagnetic linear chain. D = diamagnetic, AFM = antiferromagnetic and FM TP = ferromagnetic totally polarized.

In Fig. 3.9 is represented the transition phase diagram when starting with an antiferromagnetic linear chain.

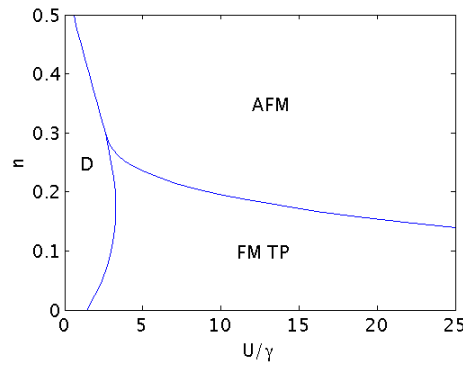


Fig. 3.9 Phase diagram for a simulation started with a totally polarized antiferromagnetic linear chain. D = diamagnetic, AFM = antiferromagnetic and FM TP = ferromagnetic totally polarized.

Finally, in Fig. 3.10 the transition phase diagram for a linear chain with a  $1s$  orbital in each lattice site, is mapped.

Something which is very interesting is that for occupations less than  $n_l^s = 0.5$ , a linear chain never converges to a ferromagnetic metallic system, but instead, it does to a half-spin metal. All the converged system labeled with FM TP are systems where the Fermi level crosses only the *majority spin* electronic band, below the bottom of the *minority spin* electronic band. An example that shows this behavior is represented on Fig. 3.11. However, a Mott transition is achieved for other configurations different of  $n_l^\sigma = 0.5$ . The transition emerges where the separation line of the areas of diamagnetic and antiferromagnetic is allocated. Then, results do not agree with Ref. [4] where it is said that this transition is typical of the half-filled limit.

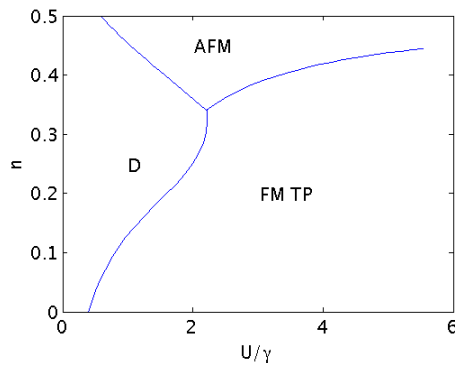


Fig. 3.10 Final phase diagram for a linear chain with only a  $1s$  state per lattice site. D = diamagnetic, AFM = antiferromagnetic and FM TP = ferromagnetic totally polarized.

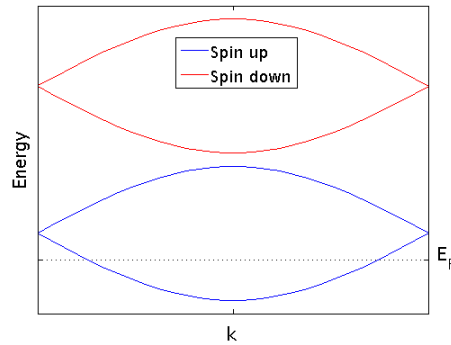


Fig. 3.11 Electronic bands for a ferromagnetic totally polarized insulator linear chain with a  $1s$  state per lattice site. Fermi energy only crosses the *majority spin* band, making the linear chain to be a so called half-spin metal.

### 3.6 Conclusions

In this chapter has been tried to reproduce the Mott transition in a 1D system and essentially obtaining that this kind of systems do not shows this behavior over values of  $U/\gamma = 0.1$ . Transition diagrams here obtained, might change if a 3D system was studied. Usually, a Mott transition emerges for  $n_{l\sigma} = 0.5$  and 3D systems with partially filled  $d$  or  $f$  shells (Ref. [1]).

# Chapter 4

## Tight-binding model under an external electric field

The study of systems out of equilibrium in condensed matter physics has been highly developed in last years because it provides rich new insights not available in equilibrium. In equilibrium, strong electronic correlations bring about a variety of phenomena such as the metal to Mott insulator transition that studied in Chapter 3. If such system is driven out of equilibrium, physics arises which remains poorly understood.

The present chapter discusses a tight-binding model under an applied electric field reviewed together with other systems out of equilibrium by Aoki et. al (Ref. [8]). A theoretical approach to study strongly correlated many-body systems is called the non-equilibrium dynamical mean-field theory (DMFT). This technique can be applied to a wide range of problems including arbitrary electromagnetic driving fields, dissipative and nondissipative systems. Here, a nondissipative system is studied.

### 4.1 Time-dependent electric fields

#### 4.1.1 Time-dependent Hamiltonian

The general lattice hamiltonian for non-dissipative models is given by

$$H(t) = - \sum_{\langle l,m \rangle} \gamma_{lm}(t) c_{l\sigma}^\dagger c_{m\sigma} + \sum_l H_{loc}^{(l)} \quad (4.1)$$

where  $l$  and  $m$  denote sites and  $\sigma$  denote spin labels. The first term is essentially the same as the tight binding hamiltonian but where the hopping is time dependent. This hopping can include

time-dependent electromagnetic fields. The second term is a sum of local interactions and single particle terms, that changes depending on which model is used. For example, for the Hubbard hamiltonian given by Eq.(3.1), this term corresponds to  $U \sum_l n_{l\uparrow} n_{l\downarrow}$ .

The model studied and developed introducing an electric field is a tight binding model, which was studied with constant hopping in Chapter 1. For this case, Eq. (4.1) transforms into

$$H(t) = - \sum_{\langle l,m \rangle} \gamma_{lm}(t) c_{l\sigma}^\dagger c_{m\sigma} \quad (4.2)$$

which corresponds with Eq. (2.21) obtained in Sec. 2.3, but written in second quantization form. For a single-band model, which also was studied in this work, the Peierls substitution introduces the vector potential  $\vec{A}(\vec{r}, t)$  as a phase factor in the hopping matrix elements

$$\gamma_{l,m}(t) = \gamma_{l,m} e^{-\frac{ie}{\hbar} \int_{\vec{R}_l}^{\vec{R}_m} d\vec{r} \cdot \vec{A}(\vec{r}, t)}. \quad (4.3)$$

Usually the applied field varies only slowly on the atomic scale, so the  $\vec{r}$  dependence of  $\vec{A}$  can be neglected. For that cases, Eq. (4.3) is transformed into

$$\gamma_{l,m}(t) = \gamma_{l,m} e^{-\frac{iea}{\hbar} \vec{A}(t)} \quad (4.4)$$

where  $a$  is the lattice spacing. So it is easily seen that the hopping is modulated by a phase. Introducing this result into Eq. (4.2) the Hamiltonian for a tight-binding model in the presence of an electric field is given by

$$H(t) = - \sum_{\langle l,m \rangle} \gamma_{lm} e^{-\frac{iea}{\hbar} \vec{A}(t)} c_{l\sigma}^\dagger c_{m\sigma}. \quad (4.5)$$

In order to follow the same notation as the used along this work, it is convenient to transform operators to momentum space by defining

$$c_{i\sigma} = \frac{1}{\sqrt{N}} \sum_{\vec{k}} e^{i\vec{k}\vec{R}_i} c_{\vec{k}\sigma} \quad (4.6)$$

where  $i = l, m$  for one-dimensional lattice of  $N$  sites,  $k_n = 2\pi n/N$  for periodic boundary conditions. For simplicity,  $a = 1$  is assumed and then, Eq. (4.5) is converted into

$$\begin{aligned}
H(t) &= \frac{-\gamma}{N} \sum_{\langle l,m \rangle} \sum_{k,k'} (e^{-\frac{ie}{\hbar}A(t)} e^{-ikl} c_{k\sigma}^\dagger e^{ik'm} c_{k'\sigma} + e^{\frac{ie}{\hbar}A(t)} e^{-ik'm} c_{k'\sigma}^\dagger e^{ikl} c_{k\sigma}) \\
&= \frac{-\gamma}{N} \sum_{l,\sigma} \sum_{k,k'} (e^{-il(k-k')} e^{i(k'-\frac{e}{\hbar}A(t))} c_{k\sigma}^\dagger c_{k'\sigma} + e^{-il(k'-k)} e^{-i(k'-\frac{e}{\hbar}A(t))} c_{k'\sigma}^\dagger c_{k\sigma}). \quad (4.7)
\end{aligned}$$

Using the fact that

$$\frac{1}{N} \sum_l e^{-il(k-k')} = \delta_{k,k'} \quad (4.8)$$

we end up with

$$\begin{aligned}
H(t) &= -\gamma \sum_{\sigma} \sum_k (e^{i(k-\frac{e}{\hbar}A(t))} c_{k\sigma}^\dagger c_{k\sigma} + e^{-i(k-\frac{e}{\hbar}A(t))} c_{k\sigma}^\dagger c_{k\sigma}) \\
&= -\gamma \sum_{\sigma,k} c_{k\sigma}^\dagger c_{k\sigma} (e^{i(k-\frac{e}{\hbar}A(t))} + e^{-i(k-\frac{e}{\hbar}A(t))}). \quad (4.9)
\end{aligned}$$

This leads to

$$H(t) = \sum_{\sigma k} \varepsilon_k(t) n_{k\sigma} \quad (4.10)$$

and

$$\varepsilon_k(t) = -2\gamma \cos(k - \frac{e}{\hbar}A(t)) \quad (4.11)$$

is the time-dependent dispersion which, for one-dimensional systems, has the form

$$\varepsilon_k(t) = \varepsilon(ka - \frac{ea}{\hbar}A(t)) \quad (4.12)$$

where  $\varepsilon(k)$  is the dispersion for zero field and  $a$  is the lattice spacing which was assumed to have a value of 1 in Eq (4.11), as Aoki et al. has obtained in Eq. (86) of Ref. [8]. Moreover, the quantity  $n_{k\sigma}$  is the occupation number for a wavevector  $k$  and spin  $\sigma$ .

### 4.1.2 Floquet matrix

When a quantum system is continuously driven by a time-periodic external force, it may enter a nonequilibrium steady state in which the overall time dependence of the system is periodic. A theoretical approach to treat periodically driven states is the Floquet method, originated from Floquet's theorem and a temporal analog of Bloch's theorem for a spatially periodic system. The advantage of using this method is that, because of the periodicity of external fields, the time-dependent problem can be converted onto a time-independent eigenvalue problem.

Floquet's theorem is a mathematical statement about the solution of an ordinary differential equation of type  $dx(t)/dt = C(t)x(t)$  where  $C(t)$  are periodic coefficients. Here, this theorem is applied to the time-dependent Schrödinger equation

$$i\frac{d}{dt}\Psi(t) = H(t)\Psi(t) \quad (4.13)$$

where  $H(t)$  is the time-dependent hamiltonian given by Eq. (4.10) and is assumed to be periodic in time with period  $T$ , so dispersion relation given by Eq. (4.11) should also comply. Floquet's theorem states that there exists a solution of Eq. (4.13) of the form

$$\Psi_a(t) = e^{-i\varepsilon_a t} u_a(t) \quad (4.14)$$

where  $u_a(t) = u_a(t+T)$  is a periodic function of  $t$ , and the real number  $\varepsilon_a$  is called the quasienergy and is unique up to integer multiples of  $\Omega = 2\pi/T$ . If one Fourier expand  $u_a(t)$  as  $u_a(t) = \sum_n e^{-in\Omega t} u_a^n$ , with each value  $u_a^n$  called the  $n$ -Floquet mode of the  $\Psi_a(t)$  state, it is obtained the so called Floquet matrix whose eigenvalues gives the quasienergy  $\varepsilon_a$ . To prove this, solution given by Eq. (4.14) is introduced into Eq. (4.13)

$$\begin{aligned} i[-i\varepsilon_a e^{-i\varepsilon_a t} u_a(t) + e^{-i\varepsilon_a t} \frac{d}{dt} u_a(t)] &= H(t) e^{-i\varepsilon_a t} u_a(t) \\ \varepsilon_a u_a(t) + i \frac{d}{dt} u_a(t) &= H(t) u_a(t). \end{aligned} \quad (4.15)$$

Introducing the Fourier expansion of the periodic function  $u_a(t)$  and deriving

$$\begin{aligned} \varepsilon_a \sum_n e^{-in\Omega t} u_a^n + i \frac{d}{dt} \sum_n e^{-in\Omega t} u_a^n &= H(t) \sum_n e^{-in\Omega t} u_a^n \\ \varepsilon_a \sum_n e^{-in\Omega t} u_a^n + \sum_n n\Omega e^{-in\Omega t} u_a^n &= H(t) \sum_n e^{-in\Omega t} u_a^n. \end{aligned} \quad (4.16)$$

Multiplying both sides by  $\frac{1}{T} \int_0^T dt e^{im\Omega t}$  Eq.(4.16) is transformed into

$$\begin{aligned} \frac{1}{T} \int_0^T dt \varepsilon_a \sum_n e^{i(m-n)\Omega t} u_a^n + \frac{1}{T} \int_0^T dt \sum_n n\Omega e^{i(m-n)\Omega t} u_a^n &= \frac{1}{T} \int_0^T dt H(t) \sum_n e^{i(m-n)\Omega t} u_a^n \\ \sum_n \varepsilon_a u_a^n \frac{1}{T} \int_0^T dt e^{i(m-n)\Omega t} + \sum_n n\Omega u_a^n \frac{1}{T} \int_0^T dt e^{i(m-n)\Omega t} &= \sum_n u_a^n \frac{1}{T} \int_0^T dt e^{i(m-n)\Omega t} H(t). \end{aligned} \quad (4.17)$$

Assuming that

$$\frac{1}{T} \int_0^T e^{i(m-n)\Omega t} dt = \delta_{mn}$$

and both substituting into Eq. (4.17)

$$\begin{aligned} \sum_n \varepsilon_a u_a^n \delta_{mn} + \sum_n n\Omega u_a^n \delta_{mn} &= \sum_n u_a^n H_{mn} \\ \sum_n (H_{mn} - n\Omega \delta_{mn}) u_a^n &= \sum_n \varepsilon_a u_a^n \delta_{mn}. \end{aligned} \quad (4.18)$$

Rewriting Eq. (4.18) to follow the same notation as in Ref. [8]

$$\sum_n (H_{mn} - n\Omega \delta_{mn}) u_a^n = \varepsilon_a u_a^m \quad (4.19)$$

that corresponds to Eq. (177) of Ref. [8] and where

$$H_{mn} = \frac{1}{T} \int_0^T e^{i(m-n)\Omega t} H(t) dt \quad (4.20)$$

is the Floquet matrix form of the Hamiltonian. Thus the quasienergies  $\varepsilon_a$  are the eigenvalues of the infinite-dimensional Floquet matrix  $H_{mn} - n\Omega \delta_{mn}$ . To avoid degeneration of  $\varepsilon_a$ , the condition  $-\Omega/2 \leq \varepsilon_a \leq \Omega/2$  is imposed and, analogously to the first Brillouin zone, this is the so called first Floquet zone. Thus, as a consequence of the Floquet theorem, the time-dependent differential equation is transformed into a time-independent problem.

## 4.2 Tight-binding model in a time-periodic electric field

To solve the problem, only  $A(t)$  needs to be defined. On Ref. [8] some results of various problems are both analyzed from a theoretical and experimental point of view. One of the theoretical studies, is the effect of time-dependent AC electric fields in correlated systems. The system reproduced in this chapter is a closed system, in which the total energy and the number of particles are conserved. The effect of AC fields has been theoretically studied for a noninteracting tight-binding model

(Dunlap and Kenkre, 1986; Holthaus, 1992) in a time-periodic electric field  $E(t) = E \cos(\Omega t)$ , for a one-dimensional problem. Having a vector potential of

$$A(t) = -E/\Omega \sin \Omega t. \quad (4.21)$$

The model can be reproduced within the Floquet theory exposed on Sec. 4.1. Introducing Eq. (4.21) on Eq. (4.10) the time-dependent hamiltonian for a 1D system is defined as

$$H(t) = -2\gamma \sum_{k\sigma} \cos [ka + E/\Omega \sin(\Omega t)] c_{k\sigma}^\dagger c_{k\sigma}. \quad (4.22)$$

Therefore, the terms of Floquet matrix are given by the solution of

$$H_{mn} - n\Omega \delta_{mn} = \frac{1}{T} \int_0^T e^{i(m-n)\Omega t} (-2\gamma \sum_{k\sigma} \cos [ka + E/\Omega \sin(\Omega t)] c_{k\sigma}^\dagger c_{k\sigma}) - n\Omega \delta_{mn}. \quad (4.23)$$

Assuming  $T = 1$  s and a unit for the lattice constant  $a$ , written in matrix form, the elements are

$$H_{mn} - n\Omega \delta_{mn} = \begin{pmatrix} -2\gamma J_0(A) \cos k & 2\gamma i J_1(A) \sin k & -2\gamma J_2(A) \cos k & \dots \\ -2\gamma i J_1(A) \sin k & -2\gamma J_0(A) \cos k - \Omega & 2\gamma i J_1(A) \sin k & \dots \\ -2\gamma J_2(A) \cos k & -2\gamma i J_1(A) \sin k & -2\gamma J_0(A) \cos k - 2\Omega & \dots \\ \vdots & \vdots & \vdots & \ddots \end{pmatrix}$$

which was solved in detail in Appendix A.4 and where  $A = \frac{E}{\Omega}$ . If we deal with 2D or 3D systems then,  $\cos k$  has to be substituted by  $\sum_a \cos k_a$  with  $a = x, y, z$ . Since  $n = 0, \pm 1, \pm 2, \dots$  and, hence,  $m = 0, \pm 1, \pm 2, \dots$ , could take negative values, it is convenient to express the Floquet matrix in a symmetric way

$$H_{mn} - n\Omega \delta_{mn} = \begin{pmatrix} \dots & \dots & \dots & \dots & \dots \\ \dots & -2\gamma J_0(A) \cos k - \Omega & 2\gamma i J_1(A) \sin k & -2\gamma J_2(A) \cos k & \dots \\ \dots & -2\gamma i J_1(A) \sin k & -2\gamma J_0(A) \cos k & 2\gamma i J_1(A) \sin k & \dots \\ \dots & -2\gamma J_2(A) \cos k & -2\gamma i J_1(A) \sin k & -2\gamma J_0(A) \cos k + \Omega & \dots \\ \dots & \dots & \dots & \dots & \dots \end{pmatrix}.$$

It is easy to see that hopping for zeroth-order Bessel function is renormalized by the periodic driving to an effective hopping that is

$$\gamma^{eff} = J_0(A) \gamma \quad (4.24)$$

in agreement with Eq. (228) of Ref. [8] and where  $\gamma$  is the hopping of the tight-binding model. Since  $J_0$  is an oscillating function, the effective hopping vanishes at the so called Bessel zeros.

### 4.3 Results

Solving Eq. (4.19) an spectrum of quasienergies  $\varepsilon_a$  is obtained. Each diagonal element of the matrix represents the static system with energies moved an absolute value of  $n\Omega$ . The  $n$ -Floquet mode is a replica which represents the static system excited because  $n$  photons absorbed (if  $n > 0$ ) or emitted (if  $n < 0$ ). The diagonalization of the hamiltonian was done numerically with the help of the Mathematica software.

As done in some of the examples presented in this work, a value of  $\gamma = 0.5$  is studied. The values introduced for the electric field was  $E = 1$  N/C and  $T = 1$  s so  $\omega = 2\pi/T = 2\pi$  rad/s. This values are arbitrary so many other values can be tried. In Fig. 4.1 the spectrum of quasienergies for a three-dimensional Floquet-matrix are plotted so three bands appear. As it can be observed they have the same cosine shape as in the tight-binding model but, little further on, it is demonstrated that is modulated by the zeroth-order Bessel function. This figure is in agreement with those of Ref. [8].

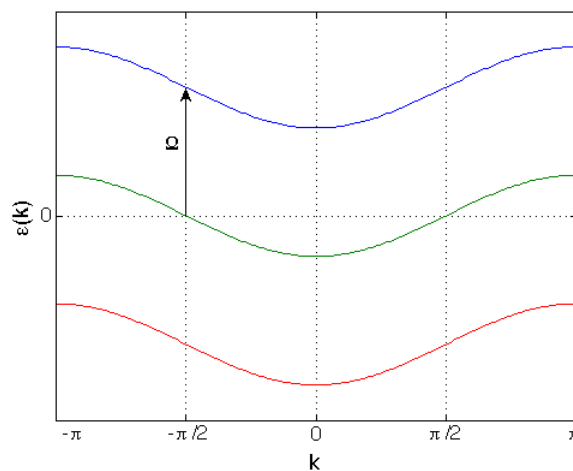


Fig. 4.1 Floquet bands of energy for a system under a periodic electric field which absorbs one photon, blue line; no photon is absorbed or emitted, green line; and emits one photon, red line. These bands are made keeping three Floquet modes.

This bands corresponds to energies given by the eigenvalues of the problem. The values of this matrix were obtained computationally but no analytic expression for this quasienergies has been derived from the calculus because of its difficulty. However, it seems to depend on more terms than

$J_0(A)$ , as the 3 order Floquet matrix depends also on  $J_2(A)$ . That assumption is not in agreement with Ref. [8], which it is said the quasienergies are exactly

$$\varepsilon_\alpha(k) = \begin{pmatrix} \dots \\ -2\gamma J_0(A) \cos k - 2\Omega \\ -2\gamma J_0(A) \cos k - \Omega \\ -2\gamma J_0(A) \cos k \\ -2\gamma J_0(A) \cos k + \Omega \\ -2\gamma J_0(A) \cos k + 2\Omega \\ \dots \end{pmatrix}. \quad (4.25)$$

If the first orders of Bessel functions are drawn like in Fig. 4.2, it is easily seen that making bigger the value of  $A$ , an interesting point is coming. That is the first zero of the *zeroth*-order Bessel function.

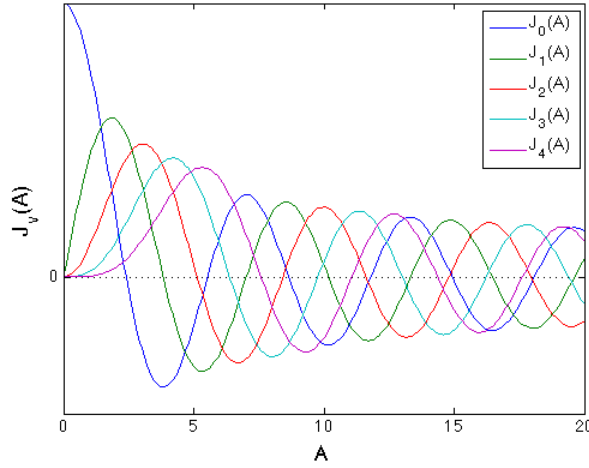


Fig. 4.2 First five Bessel functions.

On that point,  $J_0(A) = 0$  but  $J_2(A)$  has a not negligible value. If it is correctly the assumption of Ref. [8], and terms belonging other Bessel functions don't take part in the energy of the system, the quasienergies vector for 3 Floquet sectors should be given by

$$\varepsilon_\alpha = \begin{pmatrix} -\Omega \\ 0 \\ \Omega \end{pmatrix} \quad (4.26)$$

where the dependence of  $\varepsilon_\alpha$  with  $k$  is then lost and which means the effective hopping exactly vanishes for zero Floquet mode making the electrons completely localized on the atoms and then,

obtaining a transition from metal to insulator material with completely flat bands for that conditions. As the first zero of the general  $J_0(x)$  is produced at  $x = 2.40483$ , this implies that for  $E = 1$  V/m, the electric field should have a period of  $T = 15.11$  s. For this values,  $\Omega = 0.4158$  rad/s so the quasienergies should be

$$\varepsilon_\alpha = \begin{pmatrix} -0.4158 \\ 0 \\ 0.4158 \end{pmatrix}. \quad (4.27)$$

However, software mathematica and also matlab gives the following result

$$\varepsilon_\alpha = \begin{pmatrix} -0.4198 \\ 0 \\ 0.4198 \end{pmatrix} \quad (4.28)$$

values which are a bit larger than expected so it seems to have more contributions than a simple  $J_0(A)$ . If a more Floquet modes are introduced in the calculus, for example, a 7 order hamiltonian matrix, the eigenvalues are

$$\varepsilon_\alpha = \begin{pmatrix} -1.2515 \\ -0.8355 \\ -0.4159 \\ 0 \\ 0.4159 \\ 0.8355 \\ 1.2515 \end{pmatrix} \quad (4.29)$$

where it can be noticed, the values for the first Floquet modes approximates better to the solution  $\pm n\Omega$ . Many orders were tried and was observed that for orders of Floquet matrix greater than 9, solution is achieved with an absolute difference with the theoretic value of  $\pm 0.000031$ , which is not significant. So the larger the Floquet matrix, the more accurate solution and terms like  $J_2(A)$  and others, are progressively canceled. Thus, it is feasible to say that quasienergies complies Eq. (4.25).

This point could also be achieved with a period of  $T = 1$  s but  $E = 15.11$  V/m. In that case, the value of  $\Omega^2$  is the main contribution to the energies of the Floquet modes as  $\Omega = 2\pi$  rad/s whereas  $J_2(2.40483)$  will maintain the same low value. So for this case, are again the Floquet's modes with bands moved an absolute value of  $n\Omega$  the ones which governs the energy of the system, and less Floquet sectors are needed to reach the solution. In fact, the 3 order Floquet matrix directly gives the real solution. In this case, the quasienergies are

$$\varepsilon_\alpha = \begin{pmatrix} -6.3420 \\ 0 \\ 6.3420 \end{pmatrix}. \quad (4.30)$$

So it has been proven that for the first zero of  $J_0(A)$  a metal to insulator transition emerges caused by an electric field dependent on time. This effect is known as dynamical localization.

## 4.4 Conclusions

In this chapter, a simply tight-binding model including an electric field has been studied. When this electric field is time-dependent, the energies of the system are governed by the Floquet's modes. Each Floquet mode corresponds to a photon absorbed or emitted in the process. If a system emits  $n$  photons, then its band energy will be  $\varepsilon_a = -2\gamma J_0(A) \cos k - n\Omega$  plus some terms which is demonstrated are contributors that will be canceled, so it is governed by the hopping of the tight-binding model modulated by the  $J_0(A)$  Bessel function.

It was also shown how hopping vanishes at some frequencies and intensities of the electric field. That means, if one simulates a linear chain under the conditions of one of the Bessel zeros, an insulator material (dynamical localization) will emerge.

# Conclusions

To conclude this project, general lines of the observed behavior of the systems studied are here summarized.

In Chapter 2 a simple tight-binding model was studied. In relation with the hopping parameter it has been shown its relation with the band width: the more  $\gamma$  the wider bands, the metallic states are favored. Opposite, a low value of  $\gamma$  results in flatter bands, typical of insulator materials. The electronic bands simulated belongs to a  $1s$  state so a cosine shape is reproduced. The analytic formula for the energies has been obtained and with very simply simulations this shape was corroborate. At the end of this chapter, simulations with two atoms per unit cell are included and typical folded bands were drawn.

In Chapter 3 more difficult hamiltonian governs the energy of the system. The dependence of the ground state of a linear chain with three parameters have been analyzed. This three parameters are the so called hopping  $\gamma$ , Hubbard  $U$  and density of states of each spin,  $n_i^\uparrow$  and  $n_i^\downarrow$ . As the final system is linked with the relation  $U/\gamma$ , various values of this relation were reproduced for many different occupations. The conclusion of this study is that for half-filling limit and values of  $U/\gamma > 0.2$ , no Mott transition is observed. However, Mott transition is observed for other occupations and higher values of  $U/\gamma$ .

In Chapter 4 a similar hamiltonian than in Chapter 1 is used, with the difference of having a time-dependent hopping,  $\gamma(t)$ . An analytic expression of the energy for a linear chain was obtained. The energy of the system is characterized by a hopping modulated by the zero-th order Bessel function and a series of Floquet modes come out which electronic bands are allocated at energies moved upwards and downwards a quantity of  $\pm n\Omega$  where  $n$  is the  $n$ -th Floquet mode. This modes responds to energy of excited states where  $n$  photons are absorbed ( $+n\Omega$ ) or emitted ( $-n\Omega$ ).

Finally, it should be highlighted the fact that this project has been a multidisciplinary work. Concepts belonging to the quantum physics of solids studied in the degree has been firm up. This work also serves as introduction to real computational methods and its approximations, required to be able to reproduce real materials. As part of this dissertation, Chapter 4 was developed in collaboration with the Brown University. The concepts learned with the study of the tight-binding model under an external electric field includes second-quantization formalism widely used

in quantum mechanics, the usage of Mathematica software and some mathematical concepts including Floquet's theorem. This stance was also full of enriching experiences apart from this work.

# References

- [1] Anisimov, V. and Izyumov, Y. (2010). *Electronic structure of strongly correlated materials*. Springer.
- [2] Ashcroft, N. W. and Mermin, N. D. (1976). *Solid State physics*. Saunders College Publishing, Philadelphia.
- [3] Bloch, F. (1928). Über die quantenmechanik der elektronen in kristallgittern. *Z. Phys*, 52:555.
- [4] Editorial (2013). The hubbard model at half a century. *Nature Physics*, 7:523.
- [5] Grosso, G. and Parravicini, G. P. (2000). *Solid State physics*. Academic Press, London.
- [6] Gutzwiller, M. (1963). *Physical Review Letters*, 10:159–152.
- [7] Harrison, W. A. (1988). *Electronic Structure and the properties of solids*. Dover, Mineola, New York.
- [8] Hideo Aoki, Naoto Tsuji, M. E. M. K. T. O. and Werner, P. (2012). Nonequilibrium dynamical mean-field theory and its applications. *Review of Modern Physics*, 86:779–837.
- [9] Hubbard, J. (1963). *Proceedings of Royal Society of London*, A 276:237–257.
- [10] Kanamori, J. (1963). *Progress of Theoretical Physics*, 30:275–289.
- [11] Lieb, E. H. and wu, F. Y. (1968). *Physical Review Letters*, 20 25:1445–1449.
- [12] Martin, R. M. (2004). *Electronic Structure. Basic Theory and Practical Methods*. Cambridge University Press, Cambridge.
- [13] P. Garcia-Fernandez, J.C. Wojdel, J. I. and Junquera, J. (2016). Second-principles method including electron and lattice degrees. *Physical Review B*, 97.



# Appendix A

## Demonstrations

### A.1 Proof that the basis functions defined in Eq.(2.7) verify the Bloch theorem

Here it is verified that the basis function defined in Eq. (2.7) complies the property for Bloch functions shown in Eq. (2.2). With this objective the translation vector  $\vec{T}$  in Eq. (2.7) is now called  $\vec{T}'$  and  $\vec{T}$  is the one added to verify the Bloch theorem. With this new notation we are proving the Bloch theorem in a cell translated  $\vec{T}'$  from the unit cell.

$$\begin{aligned}\phi_{\mu\vec{k}}(\vec{r} + \vec{T}) &= A_{\mu\vec{k}} \sum_{\vec{T}'} e^{i\vec{k}\cdot\vec{T}'} \phi_{\mu}(\vec{r} + \vec{T} - \vec{\tau}_{\mu} - \vec{T}') \\ &= A_{\mu\vec{k}} \sum_{\vec{T}'} e^{i\vec{k}\cdot\vec{T}'} \phi_{\mu}(\vec{r} - \vec{\tau}_{\mu} - (\vec{T}' - \vec{T})).\end{aligned}\tag{A.1}$$

Now, making the change  $\vec{T}'' = \vec{T}' - \vec{T}$  (so  $\vec{T}' = \vec{T}'' + \vec{T}$ ),

$$\begin{aligned}\phi_{\mu\vec{k}}(\vec{r} + \vec{T}) &= A_{\mu\vec{k}} \sum_{\vec{T}'} e^{i\vec{k}\cdot\vec{T}'} \phi_{\mu}(\vec{r} - \vec{\tau}_{\mu} - (\vec{T}' - \vec{T})) \\ &= A_{\mu\vec{k}} \sum_{\vec{T}''} e^{i\vec{k}\cdot(\vec{T}'' + \vec{T})} \phi_{\mu}(\vec{r} - \vec{\tau}_{\mu} - \vec{T}'') \\ &= e^{i\vec{k}\cdot\vec{T}} A_{\mu\vec{k}} \sum_{\vec{T}''} e^{i\vec{k}\cdot\vec{T}''} \phi_{\mu}(\vec{r} - \vec{\tau}_{\mu} - \vec{T}'') \\ &= e^{i\vec{k}\cdot\vec{T}} \phi_{\mu\vec{k}}(\vec{r}).\end{aligned}\tag{A.2}$$
$$\tag{A.3}$$

## A.2 Derivation the factor $A_{\mu\vec{k}}$ required for the Bloch basis states $\phi_{\mu\vec{k}}(\vec{r})$ to be normalized.

If we want the Bloch basis states to be normalized, must be comply

$$\langle \phi_{\mu\vec{k}}(\vec{r}) | \phi_{\mu\vec{k}}(\vec{r}) \rangle = 1, \quad (\text{A.4})$$

where

$$\begin{aligned} \langle \phi_{\mu\vec{k}}(\vec{r}) | \phi_{\mu\vec{k}}(\vec{r}) \rangle &= \int_{\text{all space}} d\vec{r} \phi_{\mu\vec{k}}^*(\vec{r}) \phi_{\mu\vec{k}}(\vec{r}) \\ &= \int_{\text{all space}} d\vec{r} \left[ A_{\mu\vec{k}}^* \sum_{\vec{T}} e^{-i\vec{k}\cdot\vec{T}} \phi_{\mu}^*(\vec{r} - \vec{\tau}_{\mu} - \vec{T}) \right] \left[ A_{\mu\vec{k}} \sum_{\vec{T}'} e^{i\vec{k}\cdot\vec{T}'} \phi_{\mu}(\vec{r} - \vec{\tau}_{\mu} - \vec{T}') \right] \\ &= A_{\mu\vec{k}}^* A_{\mu\vec{k}} \sum_{\vec{T}} \sum_{\vec{T}'} e^{i\vec{k}\cdot(\vec{T}' - \vec{T})} \int_{\text{all space}} d\vec{r} \phi_{\mu}^*(\vec{r} - \vec{\tau}_{\mu} - \vec{T}) \phi_{\mu}(\vec{r} - \vec{\tau}_{\mu} - \vec{T}'). \end{aligned} \quad (\text{A.5})$$

Now, we can distinguish between two different cases:

- If the functions  $\phi_{\mu}(\vec{r} - \vec{\tau}_{\mu} - \vec{T})$  are orthonormal, Eq. (A.5) transforms into

$$\begin{aligned} \langle \phi_{\mu\vec{k}}(\vec{r}) | \phi_{\mu\vec{k}}(\vec{r}) \rangle &= A_{\mu\vec{k}}^* A_{\mu\vec{k}} \sum_{\vec{T}} \sum_{\vec{T}'} e^{i\vec{k}\cdot(\vec{T}' - \vec{T})} \int_{\text{all space}} d\vec{r} \phi_{\mu}^*(\vec{r} - \vec{\tau}_{\mu} - \vec{T}) \phi_{\mu}(\vec{r} - \vec{\tau}_{\mu} - \vec{T}') \\ &= |A_{\mu\vec{k}}|^2 \sum_{\vec{T}} \sum_{\vec{T}'} e^{i\vec{k}\cdot(\vec{T}' - \vec{T})} \delta_{\vec{T}, \vec{T}'} \\ &= |A_{\mu\vec{k}}|^2 \sum_{\vec{T}} 1 \\ &= |A_{\mu\vec{k}}|^2 N = 1, \end{aligned} \quad (\text{A.6})$$

and, therefore

$$A_{\mu\vec{k}} = \frac{1}{\sqrt{N}}. \quad (\text{A.7})$$

- In the general case, with non orthonormal atomic orbitals, Eq. (A.5) transforms into

$$\begin{aligned} \langle \phi_{\mu\vec{k}}(\vec{r}) | \phi_{\mu\vec{k}}(\vec{r}) \rangle &= A_{\mu\vec{k}}^* A_{\mu\vec{k}} \sum_{\vec{T}} \sum_{\vec{T}'} e^{i\vec{k} \cdot (\vec{T}' - \vec{T})} \int_{\text{all space}} d\vec{r} \phi_{\mu}^*(\vec{r} - \vec{\tau}_{\mu} - \vec{T}) \phi_{\mu}(\vec{r} - \vec{\tau}_{\mu} - \vec{T}') \\ &= |A_{\mu\vec{k}}|^2 \sum_{\vec{T}} \left( \sum_{\vec{T}'} e^{i\vec{k} \cdot (\vec{T}' - \vec{T})} \int_{\text{all space}} d\vec{r} \phi_{\mu}^*(\vec{r} - \vec{\tau}_{\mu} - \vec{T}) \phi_{\mu}(\vec{r} - \vec{\tau}_{\mu} - \vec{T}') \right) \end{aligned} \quad (\text{A.8})$$

In the sum in brackets, the translation vector  $\vec{T}$  is fixed. We can therefore make the following change of variables in the integral  $\vec{r}' = \vec{r} - \vec{T}$ ,

$$\begin{aligned} \langle \phi_{\mu\vec{k}}(\vec{r}) | \phi_{\mu\vec{k}}(\vec{r}) \rangle &= |A_{\mu\vec{k}}|^2 \sum_{\vec{T}} \left( \sum_{\vec{T}'} e^{i\vec{k} \cdot (\vec{T}' - \vec{T})} \int_{\text{all space}} d\vec{r}' \phi_{\mu}^*(\vec{r}' + \vec{T} - \vec{\tau}_{\mu} - \vec{T}) \phi_{\mu}(\vec{r}' + \vec{T} - \vec{\tau}_{\mu} - \vec{T}') \right) \\ &= |A_{\mu\vec{k}}|^2 \sum_{\vec{T}} \left( \sum_{\vec{T}'} e^{i\vec{k} \cdot (\vec{T}' - \vec{T})} \int_{\text{all space}} d\vec{r}' \phi_{\mu}^*(\vec{r}' - \vec{\tau}_{\mu}) \phi_{\mu} \left[ \vec{r}' - \vec{\tau}_{\mu} - (\vec{T}' - \vec{T}) \right] \right) \end{aligned} \quad (\text{A.9})$$

Now, making the change in variables  $\vec{T}' - \vec{T} = \vec{T}''$ ,

$$\begin{aligned} \langle \phi_{\mu\vec{k}}(\vec{r}) | \phi_{\mu\vec{k}}(\vec{r}) \rangle &= |A_{\mu\vec{k}}|^2 \sum_{\vec{T}} \sum_{\vec{T}''} e^{i\vec{k} \cdot \vec{T}''} \int_{\text{all space}} d\vec{r}' \phi_{\mu}^*(\vec{r}' - \vec{\tau}_{\mu}) \phi_{\mu}(\vec{r}' - \vec{\tau}_{\mu} - \vec{T}'') \\ &= |A_{\mu\vec{k}}|^2 N \sum_{\vec{T}''} e^{i\vec{k} \cdot \vec{T}''} \int_{\text{all space}} d\vec{r}' \phi_{\mu}^*(\vec{r}' - \vec{\tau}_{\mu}) \phi_{\mu}(\vec{r}' - \vec{\tau}_{\mu} - \vec{T}'') \\ &= |A_{\mu\vec{k}}|^2 N S_{\mu\mu}(\vec{k}) = 1, \end{aligned} \quad (\text{A.10})$$

where, according to Eq. (14.5) and Eq. (14.2) in Ref. [12],  $S_{\mu\mu}(\vec{k})$  is defined as

$$\begin{aligned} S_{\mu\mu}(\vec{k}) &= \sum_{\vec{T}} e^{i\vec{k} \cdot \vec{T}} S_{\mu\mu}(\vec{T}) \\ &= \sum_{\vec{T}} e^{i\vec{k} \cdot \vec{T}} \int_{\text{all space}} d\vec{r} \phi_{\mu}^*(\vec{r} - \vec{\tau}_{\mu}) \phi_{\mu}(\vec{r} - \vec{\tau}_{\mu} - \vec{T}). \end{aligned} \quad (\text{A.11})$$

Therefore, in the general case

$$A_{\mu\vec{k}} = \frac{1}{\sqrt{N} \sqrt{S_{\mu\mu}(\vec{k})}}. \quad (\text{A.12})$$

Many authors use the tight-binding model under the assumption of an orthogonal basis set, for instance:

- Grosso and Pastore Parravicini (page 17 of Ref. [5]): “For simplicity, we assume orthonormality of orbitals centered on different atoms; in this case, the Bloch sums are also orthonormal”.
- Harrison (page 5 of Ref. [7]): “We shall assume that the basis states are orthogonal... In the interest of conceptual simplicity, overlaps are omitted in the main text, though their effect is indicated at the few places where they are of consequence”.

That is why those authors use  $\frac{1}{\sqrt{N}}$  as the normalization factor, as can be seen in Eq. (36) of Ref. [5], or Eq. (3-19) of Ref. [7].

### A.3 Proof that the Bloch basis functions are orthonormal if the orbitals centered in different atoms are orthonormal

If we assume that the orbitals centered in different atoms, given by  $\phi_\mu(\vec{k})$  and  $\phi_\nu(\vec{k})$  are orthonormal, the normalization factor of the Bloch basis functions is  $\frac{1}{\sqrt{N}}$ , as we have seen in Sec. A.2

$$\begin{aligned} \langle \phi_{\mu\vec{k}}(\vec{r}) | \phi_{\nu\vec{k}}(\vec{r}) \rangle &= \frac{1}{N} \sum_{\vec{T}} \sum_{\vec{T}'} e^{i\vec{k} \cdot (\vec{T}' - \vec{T})} \int_{\text{all space}} d\vec{r} \phi_\mu^*(\vec{r} - \vec{\tau}_\mu - \vec{T}) \phi_\nu(\vec{r} - \vec{\tau}_\nu - \vec{T}') \\ &= \frac{1}{N} \sum_{\vec{T}} \left( \sum_{\vec{T}'} e^{i\vec{k} \cdot (\vec{T}' - \vec{T})} \int_{\text{all space}} d\vec{r} \phi_\mu^*(\vec{r} - \vec{\tau}_\mu - \vec{T}) \phi_\nu(\vec{r} - \vec{\tau}_\nu - \vec{T}') \right) \end{aligned} \quad (\text{A.13})$$

In the sum in brackets, the translation vector  $\vec{T}$  is fixed. We can therefore make the following change of variables in the integral  $\vec{r}' = \vec{r} - \vec{T}$ ,

$$\begin{aligned} \langle \phi_{\mu\vec{k}}(\vec{r}) | \phi_{\nu\vec{k}}(\vec{r}) \rangle &= \frac{1}{N} \sum_{\vec{T}} \left( \sum_{\vec{T}'} e^{i\vec{k} \cdot (\vec{T}' - \vec{T})} \int_{\text{all space}} d\vec{r}' \phi_\mu^*(\vec{r}' + \vec{T} - \vec{\tau}_\mu - \vec{T}) \phi_\nu(\vec{r}' + \vec{T} - \vec{\tau}_\nu - \vec{T}') \right) \\ &= \frac{1}{N} \sum_{\vec{T}} \left( \sum_{\vec{T}'} e^{i\vec{k} \cdot (\vec{T}' - \vec{T})} \int_{\text{all space}} d\vec{r}' \phi_\mu^*(\vec{r}' - \vec{\tau}_\mu) \phi_\nu[\vec{r}' - \vec{\tau}_\nu - (\vec{T}' - \vec{T})] \right) \end{aligned} \quad (\text{A.14})$$

Now, making the change in variables  $\vec{T}' - \vec{T} = \vec{T}''$ ,

$$\begin{aligned}
\langle \phi_{\mu\vec{k}}(\vec{r}) | \phi_{\nu\vec{k}}(\vec{r}) \rangle &= \frac{1}{N} \sum_{\vec{T}} \sum_{\vec{T}''} e^{i\vec{k}\cdot\vec{T}''} \int_{\text{all space}} d\vec{r}' \phi_{\mu}^*(\vec{r}' - \vec{\tau}_{\mu}) \phi_{\nu}(\vec{r}' - \vec{\tau}_{\nu} - \vec{T}'') \\
&= \frac{1}{N} \sum_{\vec{T}''} e^{i\vec{k}\cdot\vec{T}''} \int_{\text{all space}} d\vec{r}' \phi_{\mu}^*(\vec{r}' - \vec{\tau}_{\mu}) \phi_{\nu}(\vec{r}' - \vec{\tau}_{\nu} - \vec{T}'') \\
&= \sum_{\vec{T}''} e^{i\vec{k}\cdot\vec{T}''} \delta_{\mu\nu} \delta_{\vec{T}''0} \\
&= \delta_{\mu\nu},
\end{aligned} \tag{A.15}$$

where we have used that the atomic orbitals centered different atoms are orthonormal,

$$\int_{\text{all space}} d\vec{r}' \phi_{\mu}^*(\vec{r}' - \vec{\tau}_{\mu}) \phi_{\nu}(\vec{r}' - \vec{\tau}_{\nu} - \vec{T}'') = \delta_{\mu\nu} \delta_{\vec{T}''0} \tag{A.16}$$

## A.4 Demonstration of the Floquet matrix $H_{mn} - n\Omega\delta_{mn}$

The Hamiltonian written in terms of Floquet matrix is

$$\begin{aligned}
H_{mn} &= \frac{1}{T} \int_0^T dt e^{i(m-n)\Omega t} (-2\gamma \sum_{k\sigma} \cos[ka + E/\Omega \sin(\Omega t)] c_{k\sigma}^{\dagger} c_{k\sigma}) \\
&= \frac{-2\gamma}{T} \sum_{k\sigma} c_{k\sigma}^{\dagger} c_{k\sigma} \int_0^T dt e^{i(m-n)\Omega t} \cos[ka + E/\Omega \sin(\Omega t)]
\end{aligned} \tag{A.17}$$

Using Euler's formula for cosine

$$\begin{aligned}
H_{mn} &= \frac{-\gamma}{T} \sum_{k\sigma} c_{k\sigma}^{\dagger} c_{k\sigma} \int_0^T dt e^{i(m-n)\Omega t} (e^{i[ka + E/\Omega \sin(\Omega t)]} + e^{-i[ka + E/\Omega \sin(\Omega t)]}) \\
&= \frac{-\gamma}{T} \sum_{k\sigma} c_{k\sigma}^{\dagger} c_{k\sigma} \int_0^T dt (e^{i[(m-n)\Omega t + E/\Omega \sin(\Omega t)]} e^{ika} + e^{i[(m-n)\Omega t - E/\Omega \sin(\Omega t)]} e^{-ika})
\end{aligned} \tag{A.18}$$

Essentially, is the integral which has to be solved, so using Euler's formula for exponentials and calling  $A = \frac{E}{\Omega}$ , that integral is

$$I = \int_0^T dt (e^{i[(m-n)\Omega t + A \sin(\Omega t)]} (\cos k + i \sin k) + e^{i[(m-n)\Omega t - A \sin(\Omega t)]} (\cos k - i \sin k)) \tag{A.19}$$

Making a change in variables of the form

$$\begin{aligned}\Omega t &= \tau + \pi \\ dt &= \frac{1}{\Omega} d\tau \\ t = 0 &\rightarrow \tau = -\pi \\ t = T &\rightarrow \tau = \pi\end{aligned}$$

the integral is transformed into

$$\begin{aligned}I &= \int_{-\pi}^{\pi} d\tau (e^{i[(m-n)(\tau+\pi)+A\sin(\tau+\pi)]}(\cos k + i \sin k) + e^{i[(m-n)(\tau+\pi)-A\sin(\tau+\pi)]}(\cos k - i \sin k)) \\ &= \int_{-\pi}^{\pi} d\tau (e^{i[(m-n)(\tau+\pi)-A\sin(\tau)]}(\cos k + i \sin k) + e^{i[(m-n)(\tau+\pi)+A\sin(\tau)]}(\cos k - i \sin k)) \\ &= \int_{-\pi}^{\pi} d\tau (e^{i[(m-n)(\tau)-A\sin(\tau)]}e^{i\pi(m-n)}(\cos k + i \sin k) + e^{i[(m-n)(\tau)+A\sin(\tau)]}e^{i\pi(m-n)}(\cos k - i \sin k)) \\ &= \int_{-\pi}^{\pi} d\tau (e^{i[(m-n)(\tau)-A\sin(\tau)]}e^{i\pi(m-n)}(\cos k + i \sin k) + e^{i[(n-m)(-\tau)-A\sin(-\tau)]}e^{i\pi(m-n)}(\cos k - i \sin k))\end{aligned}\tag{A.20}$$

where in the second step of Eq. (A.20) a change is made due to trigonometrical properties of the sine,  $\sin(\tau + \pi) = -\sin(\tau)$ , and in fourth step the relation  $\sin(\tau) = -\sin(-\tau)$  is also used.

As  $\int_{-\pi}^{\pi} d\tau e^{i[(n-m)(-\tau)-A\sin(-\tau)]} = \int_{-\pi}^{\pi} d\tau e^{i[(n-m)(\tau)-A\sin(\tau)]}$  and Bessel functions are defined as

$$J_n(x) = \int_{-\pi}^{\pi} d\tau e^{(n\tau - x\sin(\tau))}$$

it can be concluded that Eq. (A.20) can be expressed as

$$I = J_{m-n}(A)e^{i\pi(m-n)}(\cos k + i \sin k) + J_{n-m}(A)e^{i\pi(m-n)}(\cos k - i \sin k)\tag{A.21}$$

taking into account the property of Bessel functions  $J_{n-m}(A) = (-1)^{m-n}J_{m-n}(A)$ , Eq. (A.21) can be simplified into

$$I = J_{m-n}(A)e^{i\pi(m-n)}[(\cos k + i \sin k) + (-1)^{m-n}(\cos k - i \sin k)]\tag{A.22}$$

Thus Floquet form of the hamiltonian is

$$H_{mn} = \frac{-\mathcal{Y}}{T}J_{m-n}(A)e^{i\pi(m-n)}[(\cos k + i \sin k) + (-1)^{m-n}(\cos k - i \sin k)]\tag{A.23}$$

where for simplicity creation and annihilation operators have been eliminated, but when sum to all  $k$  is done, it will accomplish the energy of a system.

Then elements of Floquet matrix are given by

$$H_{mn} - n\Omega\delta_{mn} = \frac{-\gamma}{T} J_{m-n}(A) e^{i\pi(m-n)} [(\cos k + i \sin k) + (-1)^{m-n}(\cos k - i \sin k)] - n\Omega\delta_{mn} \quad (\text{A.24})$$

Finally, depending on the value of  $m - n$  Eq. (A.25) could be reduced and expressed into pieces as

$$\begin{aligned} H_{mn} - n\Omega\delta_{mn} &= \frac{-2\gamma}{T} J_0(A) \cos k - n\Omega && \text{if } m = n \\ H_{mn} - n\Omega\delta_{mn} &= \frac{-2\gamma}{T} J_{|m-n|}(A) \cos k && \text{if } m - n \text{ even} \\ H_{mn} - n\Omega\delta_{mn} &= \frac{-2\gamma}{T} i J_{|m-n|}(A) \sin k && \text{if } m - n > 0 \text{ odd} \\ H_{mn} - n\Omega\delta_{mn} &= \frac{2\gamma}{T} i J_{|m-n|}(A) \sin k && \text{if } m - n < 0 \text{ odd} \end{aligned} \quad (\text{A.25})$$

Taking for simplicity values of  $\gamma = 1$  and  $T = 1$ , the matrix form of the Floquet matrix is

$$H_{mn} - n\Omega\delta_{mn} = \begin{pmatrix} -2J_0(A) \cos k - \Omega & 2iJ_1(A) \sin k & -2J_2(A) \cos k & \dots \\ -2iJ_1(A) \sin k & -2J_0(A) \cos k - 2\Omega & 2iJ_1(A) \sin k & \dots \\ -2J_2(A) \cos k & -2iJ_1(A) \sin k & -2J_0(A) \cos k - 3\Omega & \dots \\ \vdots & \vdots & \vdots & \ddots \end{pmatrix}$$



# Appendix B

## Computational equations

### B.1 Tight-binding equations

The simulations with SCALE UP to calculate the energy of the system have been made following a method described entirely on Ref. [13]. This article is quite difficult so in this section theory and equations have been summarized and simplified as much as possible to explain only the problems studied in this work. As in this section both theory and equations have been extracted from Ref. [13], this article is not referenced again.

Let's start with an introduction of the notation and some concepts used to describe the energy. On one side, the method relies on two key concepts: the *reference atomic geometry* (RAG) and the *reference electronic density* (RED). The first one is referred to the geometry of the nuclei of atoms and the second one is referred to electron density. The election of the RAG and the RED has no restrictions but some advice should be taken into account to better application of the model. For the RAG, it is usually convenient to employ the ground state structure or a high-symmetry configuration. For the RED, one might adopt a non-magnetic configuration. The system to simulate is then defined to be equal to the reference plus a small deformation. To clarify this concept, in Fig. B.1 it is shown, for a real problem which was not simulated in this work, the concept of the RED.

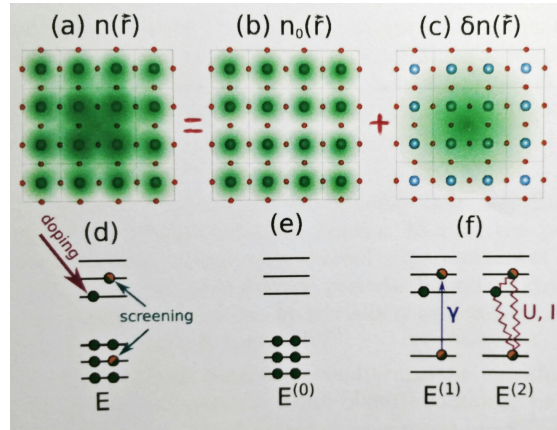


Fig. B.1 Schematic cartoon that represents the reference atomic structure and the reference and deformation electronic densities. Green balls and its green clouds represent the position of atoms and charge densities respectively. Fig. (a) represents the system to simulate while Fig. (b) and (c) represent the reference and deformation systems which when they are summed up, they form the system to simulate. In Fig. (d), (e) and (f), levels of energy are also drawn for each system.  $E$ ,  $E^{(0)}$ ,  $E^{(1)}$  and  $E^{(2)}$  are explained forward.

As the problems simulated in this work are very simple, the definition of the RED is not difficult.

On the other side, in order to allow for a more compact notation, to describe the atomic configuration, a cell/atom pair will be presented by a lowercase bold subindex, e.g. an atom  $a$  in a unit cell labeled with  $\vec{R}$  is denoted as  $\mathbf{a}$ .

Previously to see in depth which the equations to calculate the energy are, lets overview which are the steps of the self-consistent cycle that provides the energy of the final system obtained:

1. For the initial system, the one is wanted to know its energy under some specific conditions, self-consistent equation (see Sec. B.3) is solved, so eigenvalues and eigenvectors are calculated.
2. The eigenstates are filled from lower to high energies with the number of electrons of the initial system, so the occupation of each orbital is obtained.
3. The occupation provides the system for an effective potential which is calculated.
4. The effective potential is introduced into hamiltonian and again self-consistent equation (see Sec. B.3) is solved and eigenvalues and eigenvectors are calculated and, repeating step 2, occupation is again calculated.

5. The occupation of the initial system and output system given by step 4 are compared. If its difference is less than a tolerance, the self-consistence of the system is achieved. Otherwise, the cycle starts again with the new system obtained in step 4.

When self-consistence is achieved, its energy is calculated. So lets now see the equations which describe that energy. Following Eq.(5), the total energy of an atomic geometry is

$$E_{DFT} \simeq E = E^{(0)} + E^{(1)} + E^{(2)} \quad (\text{B.1})$$

where the first term,  $E^{(0)}$ , is the energy of the RED, the second term,  $E^{(1)}$ , is the one-electron excitation given by the tight-binding model in which the kinetic energy of the electrons is involved, and the third term,  $E^{(2)}$ , is the two-electron contribution and for magnetic systems, it captures the effects related with the spin polarization. In this chapter only the first and second terms are considered because are the ones related to the tight-binding model. This term is defined on Ec. (21) as

$$E = E^{(0)} + \sum_{ab} (D_{ab}^{\uparrow} + D_{ab}^{\downarrow}) \gamma_{ab} \quad (\text{B.2})$$

where  $\mathbf{a}$  and  $\mathbf{b}$  are composite indexes for atoms  $a$  and  $b$  into unit cell labeled with  $\vec{R}$ , in case of having more than one atom in the unit cell,  $D_{ab}$  is the so called deformation occupation matrix, so  $D_{ab}^{\uparrow}$  is that one for electrons with spin up and  $D_{ab}^{\downarrow}$  is the one for electrons with spin down. In general, the deformation occupation matrix, and this for each spin channel, are defined as

$$D_{ab} = d_{ab} - d_{ab}^{(0)} \quad (\text{B.3})$$

$$D_{ab}^{\uparrow} = d_{ab}^{\uparrow} - \frac{1}{2} d_{ab}^{(0)} \quad (\text{B.4})$$

$$D_{ab}^{\downarrow} = d_{ab}^{\downarrow} - \frac{1}{2} d_{ab}^{(0)} \quad (\text{B.5})$$

corresponding with Ec. (19), Ec. (30) and Ec. (31), respectively. The term  $d_{ab}$  is the density matrix and is referred in literature to as the occupation matrix, and  $d_{ab}^{(0)}$  is that of the system of reference. The expressions for this two matrix are

$$d_{ab} = \sum_{\vec{j}\vec{k}} o_{\vec{j}\vec{k}} c_{\vec{j}\vec{k}}^* c_{\vec{j}\vec{k}} e^{i\vec{k}(\vec{R}-\vec{R}')} \quad (\text{B.6})$$

$$d_{ab}^{(0)} = \sum_{\vec{j}\vec{k}} o_{\vec{j}\vec{k}}^{(0)} c_{\vec{j}\vec{k}}^{(0)*} c_{\vec{j}\vec{k}}^{(0)} e^{i\vec{k}(\vec{R}-\vec{R}')} \quad (\text{B.7})$$

in coincidence with Eq. (17) and Eq. (77). The term  $o_{\vec{j}\vec{k}}$  is the occupation of a band  $j$  for each value of wavevector  $\vec{k}$  and it is obtained from the self-consistent cycle;  $c_{\vec{j}\vec{k}}^*$ ,  $c_{\vec{j}\vec{k}}$  are the coefficients

of the Bloch wavefunctions, demonstrated forwards, of electrons moving between atoms  $a$  and  $b$  on cells labeled by  $\vec{R}$  and  $\vec{R}'$  respectively; and finally, those with a (0) upper index are referred to the system of reference.

It is very important to see that all the energies are calculated as a difference of energies between the converged system and that who is the reference. So the energies obtained in the simulation are not absolute but an increase or decrease respect to the system of reference, that is, the small deformation named before.

In the next two epigraphs coefficients of the Bloch wavefunctions have been obtained for one and two atoms per unit cell since both cases are the ones treated in this work.

### Normalization of the wavefunction with one atom per unit cell

The general form of the wavefunction is obtained from Ec. (15)

$$|\psi_{j\vec{k}}\rangle = \sum_a c_{j\vec{k}a} e^{i\vec{k}\vec{R}} |\vec{R}a\rangle \quad (\text{B.8})$$

where  $a$  is the composite index explained before that group all the atoms  $a$  into a unit cell  $\vec{R}$ .

If only one atom per unit cell is considered Eq.B.8 transforms into

$$|\psi_{j\vec{k}}\rangle = \sum_{\vec{R}} c_{j\vec{k}} e^{i\vec{k}\vec{R}} |\vec{R}\rangle \quad (\text{B.9})$$

To comply the fact that the wavefunction has to be normalized, it should be demonstrated that

$$\langle \psi_{j\vec{k}} | \psi_{j\vec{k}} \rangle = 1 \quad (\text{B.10})$$

So,

$$\begin{aligned} \langle \psi_{j\vec{k}} | \psi_{j\vec{k}} \rangle &= c_{j\vec{k}} c_{j\vec{k}}^* \sum_{\vec{R}'\vec{R}} e^{i\vec{k}(\vec{R}-\vec{R}')} \langle \vec{R} | \vec{R}' \rangle \\ &= c_{j\vec{k}} c_{j\vec{k}}^* \sum_{\vec{R}'\vec{R}} e^{i\vec{k}(\vec{R}-\vec{R}')} \delta_{\vec{R}\vec{R}'} \\ &= c_{j\vec{k}} c_{j\vec{k}}^* \sum_{\vec{R}'\vec{R}} 1 \\ &= |c_{j\vec{k}}|^2 N \end{aligned} \quad (\text{B.11})$$

Finally,

$$\begin{aligned} |c_{j\vec{k}}|^2 N &= 1 \\ c_{j\vec{k}} &= \frac{1}{\sqrt{N}} \end{aligned} \quad (\text{B.12})$$

Where  $N$  is the number of unit cells that forms the solid.

### Normalization of the wavefunction with two atom per unit cell

It is interesting to see which are the coefficients of the wavefunction to be normalized as the problem solved in the next chapter is required to have two atoms per cell, as will be shown later. Based on Eq. (B.8), if atoms  $a$  and  $b$  are located in the same unit cell labeled by  $\vec{R}$ , the wavefunction is

$$\begin{aligned} |\psi_{j\vec{k}}\rangle &= \sum_{\vec{R}} c_{ja\vec{k}} e^{i\vec{k}\vec{R}} |\vec{R}a\rangle + c_{jb\vec{k}} e^{i\vec{k}\vec{R}} |\vec{R}b\rangle \\ &= c_{j\vec{k}} \sum_{\vec{R}} e^{i\vec{k}\vec{R}} (|\vec{R}a\rangle + |\vec{R}b\rangle) \end{aligned} \quad (\text{B.13})$$

where it has been assumed that  $c_{ja\vec{k}} = c_{jb\vec{k}}$  as its represents coefficients of linear combination of functions. To normalize the wavefunction given by Eq. (B.13) it has to comply the same condition as in Eq. (B.10). So

$$\begin{aligned} \langle \psi_{j\vec{k}} | \psi_{j\vec{k}} \rangle &= c_{j\vec{k}}^* c_{j\vec{k}} \sum_{\vec{R}\vec{R}'} e^{i\vec{k}(\vec{R}-\vec{R}')} (\langle \vec{R}'a | + \langle \vec{R}'b |) (|\vec{R}a\rangle + |\vec{R}b\rangle) \\ &= c_{j\vec{k}}^* c_{j\vec{k}} \sum_{\vec{R}\vec{R}'} e^{i\vec{k}(\vec{R}-\vec{R}')} (\langle \vec{R}'a | \vec{R}a\rangle + \langle \vec{R}'b | \vec{R}a\rangle + \langle \vec{R}'a | \vec{R}b\rangle + \langle \vec{R}'b | \vec{R}b\rangle) \\ &= c_{j\vec{k}}^* c_{j\vec{k}} \sum_{\vec{R}\vec{R}'} e^{i\vec{k}(\vec{R}-\vec{R}')} (\langle \vec{R}'a | \vec{R}a\rangle + \langle \vec{R}'b | \vec{R}b\rangle) \\ &= c_{j\vec{k}}^* c_{j\vec{k}} \sum_{\vec{R}\vec{R}'} e^{i\vec{k}(\vec{R}-\vec{R}')} (\delta_{\vec{R}\vec{R}'} + \delta_{\vec{R}\vec{R}'}) \\ &= 2c_{j\vec{k}}^* c_{j\vec{k}} \sum_{\vec{R}\vec{R}'} 1 \\ &= |c_{j\vec{k}}|^2 2N \end{aligned} \quad (\text{B.14})$$

Finally,

$$\begin{aligned} |c_{j\vec{K}}|^2 2N &= 1 \\ c_{j\vec{K}} &= \frac{1}{\sqrt{2N}} \end{aligned} \quad (\text{B.15})$$

### B.1.1 One atom per unit cell

The notation when one atom per unit cell is considered, is drawn in Fig. B.2.

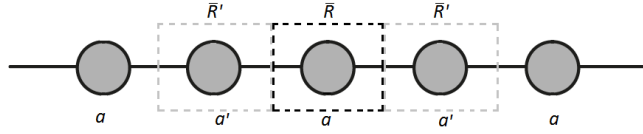


Fig. B.2 Sketch of the notation followed to solve the energy of a linear chain with one electron per atom and one atom per unit cell. The interaction between electrons is through the hopping  $\gamma$  from  $a$  atom in cell  $\vec{R}$  and its first neighbors  $a'$  in cells  $\vec{R}'$

And the distance between atoms is also  $a$ .

Detailed steps to calculate the energy for the converged system are done in this section.

The consideration of having a hopping between first neighbors leads to a hopping matrix that only has non-zero elements on the crossing terms

$$\gamma_{aa} = 0 \quad / \quad \gamma_{aa'} = \gamma \quad / \quad \gamma_{a'a} = \gamma \quad / \quad \gamma_{bb} = 0$$

that means only electrons which are jumping between atoms has one-electron energy. With this data and following Eq. (B.2) the one-electron energy is

$$\begin{aligned} E^{(1)} &= \sum_{ab} (D_{ab}^{\uparrow} + D_{ab}^{\downarrow}) \gamma_{ab} = \sum_{ab} D_{ab} \gamma_{ab} \\ &= [D_{aa} \gamma_{aa}]^{\text{onsite}} + [D_{aa'} \gamma_{aa'}]^{\text{rightcell}} + [D_{a'a} \gamma_{a'a}]^{\text{leftcell}} \end{aligned} \quad (\text{B.16})$$

because the electrons have no spin polarization. As in this problem  $\gamma_{aa} = 0$ ,  $D_{aa'} = D_{a'a}$  and  $\gamma_{aa'} = \gamma_{a'a}$  Eq. (B.16) transforms into

$$E^{(1)} = 2D_{aa'} \gamma_{aa'} \quad (\text{B.17})$$

Moreover, based on Eq. (B.3), it is easily obtained the deformation density term

$$D_{aa'} = d_{aa'} - d_{aa'}^{(0)} \quad (\text{B.18})$$

### B.1.2 Two atoms per unit cell

The notation when two atoms per unit cell are considered, is drawn in Fig. B.3.

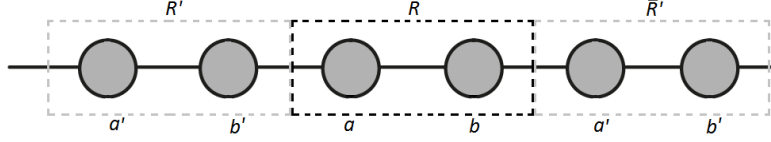


Fig. B.3 Sketch of the notation followed to solve the energy of a linear chain with one electron per atom and two atoms per unit cell. The interaction between electrons is through the hopping  $\gamma$  from  $a$  atom in cell  $\vec{R}$  and its first neighbors,  $b$  in the same cell and  $b'$  in cell  $\vec{R}'$  to the left. It should be summed up also the interaction between atom  $b$  in cell  $\vec{R}$  to its first neighbors,  $a$  in the same cell and  $a'$  in cell  $\vec{R}'$  to the right.

And the distance between atoms is again  $a$ , so the width of the cell becomes  $2a$ .

Similarly to the previous case, the one-electron energy is calculated with a configuration of two atoms per unit cell. Based again on Eq. (B.2), this energy is transformed into

$$\begin{aligned}
 E^{(1)} &= \sum_{ab} (D_{ab}^{\uparrow} + D_{ab}^{\downarrow}) \gamma_{ab} = \sum_{ab} D_{ab} \gamma_{ab} \\
 &= [D_{aa} \gamma_{aa}]^{onsite} + [D_{ab} \gamma_{ab}]^{onsite} + [D_{ba} \gamma_{ba}]^{onsite} + [D_{bb} \gamma_{bb}]^{onsite} \\
 &\quad + [D_{ba} \gamma_{ba}]^{rightcell} \\
 &\quad + [D_{ab} \gamma_{ab}]^{leftcell}
 \end{aligned} \tag{B.19}$$

where, although all the atoms are equal, the so called  $b$  is related to the second atom into the unit cell and located on the right of atom labeled  $a$  as shown in Fig. B.3 for easy understanding.

As the problem is the same than the one-electron per unit cell developed a few lines up,  $D_{ab} = D_{ba}$  independently of the cell and the same hopping is acting. Therefore, Eq. (B.19) is simplified into

$$E^{(1)} = 4D_{ab} \gamma_{ab} \tag{B.20}$$

solution which is essentially the same as obtained on the example done before but multiplied by two because of the same reason than explained before.

## B.2 Hubbard model equations

As done in Sec.B.1 lets now see the equations which describe the energy when the Hubbard model wants to be reproduced in a solid with spin polarization.

Just remembering which terms are heading on the total energy of a system, lets rewrite Eq. (5)

$$E_{DFT} \simeq E = E^{(0)} + E^{(1)} + E^{(2)} \quad (\text{B.21})$$

In this chapter is the third term, the two-electron contribution for magnetic systems  $E^{(2)}$ , the one added to the total energy saw in previous chapter. Taking into account Eq. (39) the total energy of a system considering the Hubbard interaction is defined on Ec.(66) that is

$$E = E^{(0)} + \sum_{ab} (D_{ab}^{\uparrow} + D_{ab}^{\downarrow}) \gamma_{ab} + \frac{1}{2} \sum_a \sum_{b \ a/b'} (D_{ab}^{\uparrow} + D_{ab}^{\downarrow}) (D_{a'b'}^{\uparrow} + D_{ab}^{\downarrow}) U_{aba'b'} - (D_{ab}^{\uparrow} - D_{ab}^{\downarrow}) (D_{a'b'}^{\uparrow} - D_{ab}^{\downarrow}) I_{aba'b'} \quad (\text{B.22})$$

where  $a'$  and  $b'$  indicates two atoms in a sublattice, in the case of having more than one grid and more than one atom in the unit cell. Moreover, the value of  $U_{aba'b'}$  and  $I_{aba'b'}$  are the two-electron interaction constants and, when a Hubbard model is performed, they are related with the Hubbard  $U$  through the expression

$$U = U_{aba'b'} = I_{aba'b'} \quad (\text{B.23})$$

$D_{a'b'}$ ,  $D_{a'b'}^{\uparrow}$  and  $D_{a'b'}^{\downarrow}$  has the same meaning as explained on Sec. B.1 on Eq. (B.2). Although the one-electron energy,  $E^{(1)}$ , do not capture any effect related with the spin polarization for a non-magnetic RED, it should be rewritten as a sum of spin-dependent deformation density matrix to consider magnetic RED.

For a system with zero overlapping between orbitals, zero on-site term and hopping given by the matrix

$$\gamma_{aa} = 0 \quad / \quad \gamma_{ab} = \gamma \quad / \quad \gamma_{ba} = \gamma \quad / \quad \gamma_{bb} = 0$$

So only hopping with first neighbors is consider. With this data and following Eq. (B.22) the one-electron energy is

$$\begin{aligned}
E^{(1)} &= \sum_{ab} (D_{ab}^{\uparrow} + D_{ba}^{\downarrow}) \gamma_{ab} \\
&= [(D_{aa}^{\uparrow} + D_{aa}^{\downarrow}) \gamma_{aa}]^{onsite} + [(D_{ab}^{\uparrow} + D_{ab}^{\downarrow}) \gamma_{ab}]^{onsite} \\
&+ [(D_{ba}^{\uparrow} + D_{ba}^{\downarrow}) \gamma_{ba}]^{onsite} + [(D_{bb}^{\uparrow} + D_{bb}^{\downarrow}) \gamma_{bb}]^{onsite} \\
&+ [(D_{ba}^{\uparrow} + D_{ba}^{\downarrow}) \gamma_{ba}]^{rightcell} \\
&+ [(D_{ab}^{\uparrow} + D_{ab}^{\downarrow}) \gamma_{ab}]^{leftcell}
\end{aligned} \tag{B.24}$$

For the case here simulated Eq. (B.24) can be reduced to only one term in view of the fact that  $D_{ba}^{\uparrow} = D_{ab}^{\uparrow}$  and also equal independently on which cell are located  $a$  and  $b$  atoms. The same happens for spin down deformation density matrix. Taking this into account and replacing the values of the matrix of hopping, Eq. (B.24) transforms into

$$E^{(1)} = \sum_{ab} (D_{ab}^{\uparrow} + D_{ba}^{\downarrow}) \gamma_{ab} = 4(D_{ab}^{\uparrow} + D_{ab}^{\downarrow}) \gamma_{ab} \tag{B.25}$$

Similarly, the two-electron energy is calculated. Based again on Eq. B.22, this energy is transformed into

$$E^{(2)} = \frac{1}{2} \sum_{ab} [(D_{ab}^{\uparrow} + D_{ab}^{\downarrow})(D_{ab}^{\uparrow} + D_{ab}^{\downarrow}) U_{abab} - (D_{ab}^{\uparrow} - D_{ab}^{\downarrow})(D_{ab}^{\uparrow} - D_{ab}^{\downarrow}) I_{abab}] \tag{B.26}$$

because there is only one lattice. As Hubbard  $U$  is only considered if both electrons are in the same atom. As in our chain exists two atoms, Eq. (B.27) is

$$\begin{aligned}
E^{(2)} &= \frac{1}{2} [(D_{aa}^{\uparrow} + D_{aa}^{\downarrow})(D_{aa}^{\uparrow} + D_{aa}^{\downarrow}) U_{aaaa} - (D_{aa}^{\uparrow} - D_{aa}^{\downarrow})(D_{aa}^{\uparrow} - D_{aa}^{\downarrow}) I_{aaaa}] \\
&+ \frac{1}{2} [(D_{bb}^{\uparrow} + D_{bb}^{\downarrow})(D_{bb}^{\uparrow} + D_{bb}^{\downarrow}) U_{bbbb} - (D_{bb}^{\uparrow} - D_{bb}^{\downarrow})(D_{bb}^{\uparrow} - D_{bb}^{\downarrow}) I_{bbbb}]
\end{aligned} \tag{B.27}$$

Knowing that Hubbard- $U$  is related with the parameters  $U_{bbbb}$  and  $I_{bbbb}$  as in Eq. (B.23), the energy of having two electrons on the same atom is given by

$$E^{(2)} = 2(D_{aa}^{\uparrow} D_{aa}^{\downarrow}) U + 2(D_{bb}^{\uparrow} D_{bb}^{\downarrow}) U \tag{B.28}$$

Where it can be observed that this two-electron energy only counts if both electrons are located in the same atom as Hubbard model requires.

### B.3 Self-consistent equations

The self-consistent conditions used in the second-principles method of the article are analogous to the Kohn-Sham equations

$$\sum_b h_{ab,\vec{k}}^s c_{jb,\vec{k}}^s = \varepsilon_{j\vec{k}}^s c_{ja,\vec{k}}^s, \quad (\text{B.29})$$

where  $\varepsilon_{j\vec{k}}^s$  is the  $j$ -th band energy at wavevector  $\vec{k}$  for the spin channel  $s$ . The corresponding Hamiltonian matrix,  $h_{ab,\vec{k}}^s$ , is

$$h_{ab,\vec{k}}^s = \sum_{\vec{R}_B - \vec{R}_A} e^{i\vec{k}(\vec{R}_B - \vec{R}_A)} h_{ab}^s, \quad (\text{B.30})$$

where  $h_{ab}^s$  is the real space hamiltonian.

As it was shown, total energy depends on the deformation occupation matrix  $D_{ab}^s$  for each spin channel  $s$ . This matrix is guessed in a first step of a self-consistent cycle to compute the corresponding real space Hamiltonian  $h_{ab}^s$ , and from the diagonalization of this matrix, a new deformation occupation matrix is used as input of the next iteration step. For each spin channel, the hamiltonian in real space is

$$h_{ab}^s = \gamma_{ab} + \sum_{a'b'} [(D_{ab}^s + D_{a'b'}^{-s}) U_{aba'b'} - (D_{ab}^s - D_{a'b'}^{-s}) I_{aba'b'}] \quad (\text{B.31})$$

Then, taking into account the same assumptions as before, the on-site matrix element for the up spin channel is

$$\begin{aligned} h_{aa}^\uparrow &= \gamma_{ab} + \sum_{a'b'} [(D_{ab}^\uparrow + D_{a'b'}^\downarrow) U \delta_{ab} \delta_{a'b'} \delta_{bb'} - (D_{ab}^\uparrow - D_{a'b'}^\downarrow) U \delta_{ab} \delta_{a'b'} \delta_{bb'}] \\ &= \alpha + (D_{aa}^\uparrow + D_{aa}^\downarrow) U - (D_{aa}^\uparrow - D_{aa}^\downarrow) U \\ &= \alpha - [D_{aa}^\uparrow - (-D_{aa}^\uparrow)] U \\ &= \alpha - 2D_{aa}^\uparrow U \end{aligned} \quad (\text{B.32})$$

Considering that a value of  $\alpha$  is chosen to be zero in Chapter 2, the hamiltonian diagonal elements are

$$h_{aa}^\uparrow = -2D_{aa}^\uparrow U \quad (\text{B.33})$$

Analogously

$$h_{aa}^{\downarrow} = -2D_{aa}^{\downarrow}U \quad (\text{B.34})$$

If the same process is followed for the down spin channel,

$$h_{bb}^{\uparrow} = -2D_{bb}^{\uparrow}U \quad (\text{B.35})$$

and

$$h_{bb}^{\downarrow} = -2D_{bb}^{\downarrow}U \quad (\text{B.36})$$

For crossing terms, the hamiltonian in real space is easily obtained as no  $U$  counts, so

$$h_{ab}^{\uparrow} = h_{ba}^{\uparrow} = \gamma_{ab} = \gamma \quad (\text{B.37})$$

and

$$h_{ab}^{\downarrow} = h_{ba}^{\downarrow} = \gamma_{ab} = \gamma \quad (\text{B.38})$$

### Ferromagnetic systems

Because all the sites are analogous,  $D_{aa}^{\uparrow} = D_{bb}^{\uparrow}$  and  $D_{aa}^{\downarrow} = D_{bb}^{\downarrow}$ . Moreover, due to conservation energy, it must comply  $D_{aa}^{\uparrow} = -D_{aa}^{\downarrow}$ , as the increases of the density of one spin, should accompany the same quantity of a decrease of the other spin. So, the hamiltonian in real space for the up spin, according to Eq.(B.33), Eq. (B.35) and Eq.(B.37) is formed by

$$h_{aa}^{\uparrow} = -2D_{aa}^{\uparrow}U \quad / \quad h_{bb}^{\uparrow} = -2D_{aa}^{\uparrow}U \quad / \quad h_{ba}^{\uparrow} = \gamma \quad (\text{B.39})$$

and, for the down spin channel, according to Eq.(B.34), Eq. (B.36) and Eq.(B.38) is

$$h_{aa}^{\downarrow} = 2D_{aa}^{\uparrow}U \quad / \quad h_{bb}^{\downarrow} = 2D_{aa}^{\uparrow}U \quad / \quad h_{ba}^{\downarrow} = \gamma \quad (\text{B.40})$$

## Antiferromagnetic systems

Now not all the sites are analogous, but some similarities could be established. According to the sketch of an antiferromagnetic system (Fig. 3.1g),  $D_{aa}^\uparrow = D_{bb}^\downarrow$  and  $D_{aa}^\downarrow = D_{bb}^\uparrow$ . Again, due to conservation energy, it must comply  $D_{aa}^\uparrow = -D_{aa}^\downarrow$ , as the increases of the density of one spin, should accompany the same quantity of a decrease of the other spin. Same occurs for the opposite spin. So, the hamiltonian in real space for the up spin can be rewritted in terms of  $D_{aa}^\uparrow$  that, according to (B.33), Eq. (B.35) and Eq.(B.37), is formed by

$$h_{aa}^\uparrow = -2D_{aa}^\uparrow U \quad / \quad h_{bb}^\uparrow = 2D_{aa}^\uparrow U \quad / \quad h_{ba}^\uparrow = \gamma \quad (\text{B.41})$$

and, for the down spin channel, according to Eq.(B.34), Eq. (B.36) and Eq.(B.38) is

$$h_{aa}^\downarrow = 2D_{aa}^\uparrow U \quad / \quad h_{bb}^\downarrow = -2D_{aa}^\uparrow U \quad / \quad h_{ba}^\downarrow = \gamma \quad (\text{B.42})$$

## Appendix C

### Comparison of the energies for converged systems with occupation $n_l^\sigma \neq 0.5$

In Chapter 3 a transition diagram for a linear chain with different occupations has been mapped. In order to be able to do it, for each occupation, energies of a simulation of a ferromagnetic linear chain should be compared to those of the antiferromagnetic linear chains.

In Fig. C.1, energies of a density of  $n_l^\uparrow = 0.1$  and  $n_l^\downarrow = 0.1$  states of the *majority spin* and *minority spin* respectively, are plotted. In this case, both energies coincide for almost all the values of  $U/\gamma$ . In fact, if transition diagram for both magnetic linear chains is consulted (Fig. 3.8 and Fig. 3.9), one can realized that both systems converges to the same ferromagnetic totally polarized configuration.

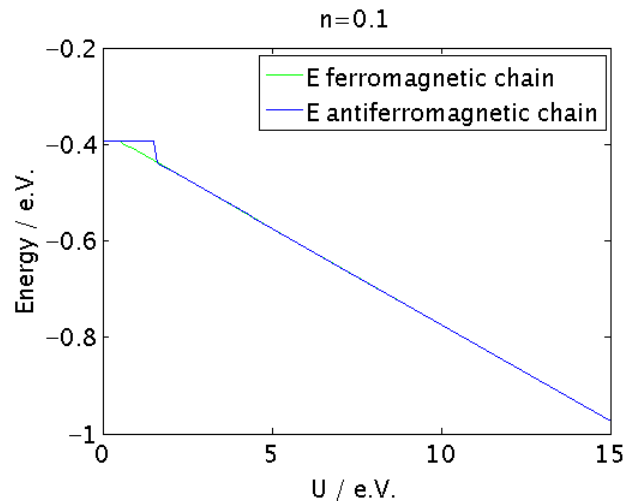


Fig. C.1 Comparison between the energy of the converged system in a ferromagnetic and antiferromagnetic linear chain simulations for  $n_l = 0.1$ .

In Fig. C.2, energies of a density of  $n_l^\uparrow = 0.2$  and  $n_l^\downarrow = 0.2$  states of the *majority spin* and *minority spin* respectively, are plotted. In this example, energies for antiferromagnetic linear chain suffer an unexpected hop to highest energies. This estrange behavior could have it origin in many reasons, e.g. a too larger value of the threshold for low values of  $U/\gamma$ . Anyway this break on the energies is not important in the final result as the energy for the antiferromagnetic linear chain is larger than the ferromagnetic one, so this last controls the resulting state.

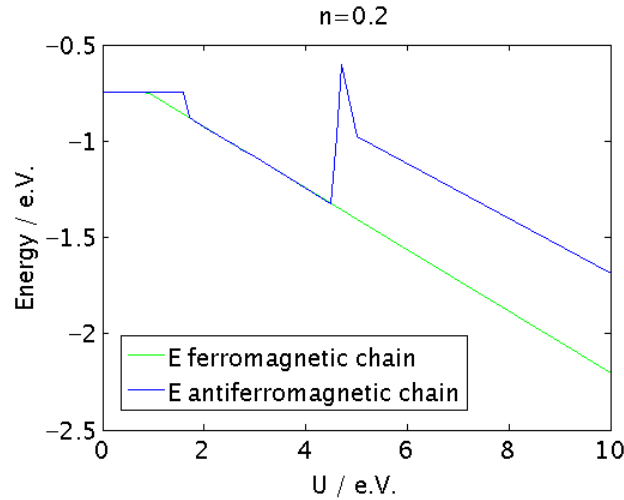


Fig. C.2 Comparison between the energy of the converged system in a ferromagnetic and antiferromagnetic linear chain simulations for  $n_l = 0.2$ .

In Fig. C.3, energies of a density of  $n_l^\uparrow = 0.3$  and  $n_l^\downarrow = 0.3$  states of the *majority spin* and *minority spin* respectively, are plotted. For this case, clearly the energies coming from the simulations of a ferromagnetic linear chain are less than for an antiferromagnetic linear chain. Because of that, the converged systems are considered to be the ones of the transition phase diagram for a ferromagnetic linear chain (Fig. 3.8).

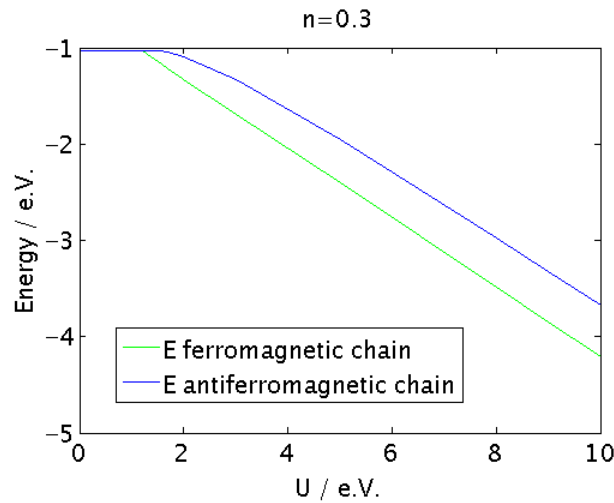


Fig. C.3 Comparison between the energy of the converged system in a ferromagnetic and antiferromagnetic linear chain simulations for  $n_l = 0.3$ .

In Fig. C.4, energies of a density of  $n_l^\uparrow = 0.35$  and  $n_l^\downarrow = 0.35$  states of the *majority spin* and *minority spin* respectively, are plotted. A small peak more energetic seems to appear for a small range of energies of a ferromagnetic linear chain. Until achieve the cross point between the two energy lines an antiferromagnetic linear chain governs the energy of the converged system. It is important to highlight that this point is not exactly obtained.

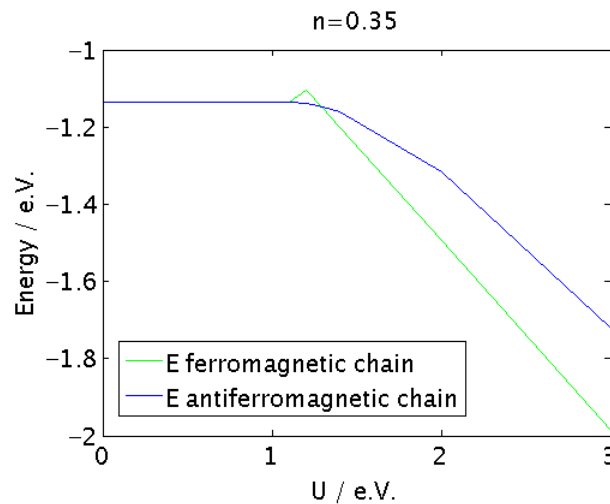


Fig. C.4 Comparison between the energy of the converged system in a ferromagnetic and antiferromagnetic linear chain simulations for  $n_l = 0.35$ .

The same holds for energies of a density of  $n_l^\uparrow = 0.4$  and  $n_l^\downarrow = 0.4$  states and also for  $n_l^\uparrow = 0.45$  and  $n_l^\downarrow = 0.45$ , where it is clearly seen that this point is moved to high values of  $U/\gamma$  when

increasing the occupation. In fact, as is plotted in Chapter 3 (Fig. 3.7), low energies for an antiferromagnetic linear chain simulations are achieved in all the range of  $U/\gamma$  simulated.

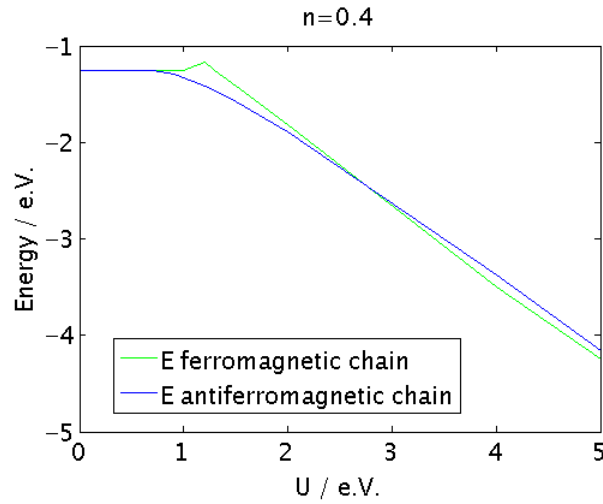


Fig. C.5 Comparison between the energy of the converged system in a ferromagnetic and antiferromagnetic linear chain simulations for  $n_l = 0.4$ .

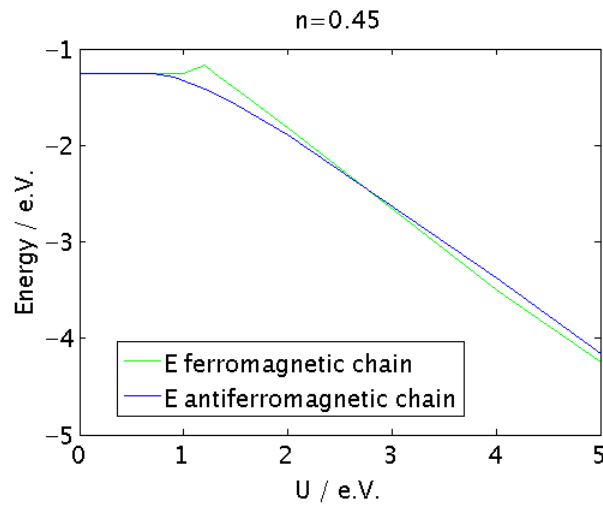


Fig. C.6 Comparison between the energy of the converged system in a ferromagnetic and antiferromagnetic linear chain simulations for  $n_l = 0.45$ .